HIGHER ORDER EFFECTS IN THE EXCITATION AND IONIZATION OF ATOMS BY FAST HEAVY CHARGED PARTICLES

by

Kenneth Wayne Hill, Sr.

A Dissertation submitted to the faculty of the University of North Carolina in partial fulfillment of the requirements for the degree of Doctor of Philosophy in the Department of Physics and Astronomy.

Chapel Hill

1974

Approved by:

_____
Adviser

_____
Reader

_____
Reader

KENNETH WAYNE HILL, SR. Higher Order Effects in the Excitation and Ionization of Atoms by Fast Heavy Charged Particles (Under the direction of EUGEN MERZBACHER).

Two topics relating to inelastic collisions of a heavy, fast particle of charge $Z_1 e$ with an atom are treated: 1) contributions to the mean energy loss of the projectile and excitation probabilities of the atom due to polarization of the electronic orbitals, and 2) cross sections for multiple ionization of the atom.

The polarization or "Z_1^3 effect" is treated in a semiclassical formulation. The incident projectile follows a straight-line trajectory and interacts with an electron bound isotropically and harmonically in a quantum-mechanical target atom. The Z_1^3 contributions to the mean energy loss and excitation probabilities are calculated for distant-collision dipole and quadrupole terms in a multipole expansion of the interaction. The dipole (E1) interaction is treated exactly, and the quadrupole (E2) term is treated in perturbation theory. Reasonable agreement is obtained with measured Z_1^3 contributions to the K-shell ionization probability of aluminum by H, D, He, and Li ions.

Cross sections for multiple ionization are determined both theoretically and experimentally. The theoretical treatment involves extension of calculations of first-order semiclassical Coulomb excitation probabilities and cross sections by means of a statistical binomial distribution. For preliminary calculations, atomic wavefunctions are approximated by isotropic harmonic oscillator states.

The experimental work involved bombardment of a thick titanium target with μA beams of H, He, Li, C, and O ions in the energy range of one to five MeV/amu. Titanium Kα diagram and satellite x rays were energy

analyzed by means of a Bragg crystal spectrometer. From two to five major x-ray lines are observed at six eV resolution, corresponding to an initial K-shell vacancy and zero to four additional L-shell vacancies. As projectile atomic number Z_1 increases, satellite intensities increase markedly and new lines appear, indicating an increasing probability of L-shell ionization. The dependence of x-ray intensities upon Z_1 and projectile energy agrees roughly with theoretical calculations. Centroid energies and widths of the x-ray peaks increase a) with increasing Z_1 and b) with increasing satellite order n (number of L-shell vacancies). Energy shifts as measured from the fluorescence spectrum energies of 4509 and 4533 eV for the diagram and first satellite lines range up to 8 eV and increase approximately linearly with Z_1 at a rate of ~ 1 eV/Z. Widths range from 10 to 37 eV and for a given satellite increase at a rate of 0.6 - 0.7 eV/Z, while for a given projectile the widths increase at 1.5 - 1.8 eV/n. Both energy shifts and increases in peak widths have been attributed mainly to an increasing degree of M-shell ionization. Comparisons of measured shifts with Hartree-Fock energy calculations show that there are one to four M-shell (3s and 3p) vacancies. Other possible explanations for increased widths are 1) an increasing spread in the possible K x-ray energies resulting from different distributions of vacancies in both the L- and M-shells, 2) increasing multiplet structure for $0 \leq n \leq 3$, and 3) Doppler shifting of the x rays due to recoil of the target atom.

ACKNOWLEDGEMENTS

The author would like to thank his research adviser, Professor Eugen Merzbacher, for his guidance throughout the duration of this work. Also, gratefully acknowledged is the support of this research by a National Defense Education Act Fellowship and by the United States Atomic Energy Commission under contract AT-(40-1)-2408.

The experimental portion of the work described herein was performed under the guidance of and in collaboration with Professor Stephen M. Shafroth, and the author gratefully acknowledges his contribution to the research. The Hartree-Fock energy calculations were provided by Dr. Don H. Madison, who also contributed through many helpful and stimulating discussions. Acknowledgement is due also to Mr. Jiun-tsong Wu for helpful discussions relating to cross section calculations and to Mr. Barney L. Doyle for contributions in the areas of data accumulation and analysis.

Finally, the author is especially indebted to his wife and children for their support and encouragement throughout his period of study and for their tolerance of his neglect and of material sacrifice.

TABLE OF CONTENTS

Chapter 1

INTRODUCTION

In recent years significant advances have been made in theoretical and experimental studies of the interactions of heavy charged particles with matter. New experiments and improved experimental technology have greatly increased the usefulness of heavy particle bombardments as a probe for studying the properties of matter. This has led to improved tests of theory resulting in the discovery of previously undetected deviations of experiment from theory. New theories have been formulated as a result of attempts to explain these deviations. These theories have met with partial success. They have led to an improved understanding of the interactions involved in ion-atom collisions. Both the improved experimental technology and the ensuing improvements in theory have sparked a rapidly growing increase in interest in ion-atom collisions. In this thesis we examine two areas of ion-atom collision theory which have recently received increased attention.

The excitation or ionization of an atom resulting from a collision between a charged particle and the atom may be described in terms of two or three basic formulations. These are the impact-parameter treatment [1], the quantum mechanical scattering approach, and the binary encounter approximation (BEA) [2].

In the impact-parameter treatment the incident charged particle follows a prescribed classical trajectory corresponding to an impact

parameter b as shown in Fig. 1. The problem may be divided into two parts. One involves the description of the projectile motion and the interaction of the charged projectile with the atomic electrons. The second part involves the description of the atom, i.e., the binding of the electrons to the atomic nucleus. The projectile-electron interaction may usually be treated as a time-dependent perturbation on the atomic states. The classical description of the projectile is valid only if its de Broglie wavelength is smaller than atomic dimensions. Thus, it is best suited for describing heavy fast projectiles. The atom may be described either by classical [3] or quantum mechanics [1,4]. The latter case is appropriately called the semiclassical approximation (SCA). A classical treatment might simplify the mathematical description of the collision problem. However, if the quantities of interest depend upon the detailed quantum mechanical nature of the atom, e.g., for subshell excitation cross sections, a classical atomic description would not be adequate.

An advantage of the impact-parameter treatment is that one can determine which range of impact parameters is the most important in the excitation being treated. If, e.g., distant collisions afford the major contribution, then the problem may be simplified by an appropriate multipole expansion of the projectile-electron interaction.

The quantum-mechanical scattering treatment is the most rigorous. It is valid, in principle, for any type of collision problem. In fact, it is the only valid approach for solving some types of problems, such as low energy electron-atom collisions. The price one must pay for rigor, however, is increased mathematical complexity. The Born approximation [5] is one simplification which has met with widespread use.

The BEA is formulated in terms of Rutherford scattering of the incident projectile by a free electron having some initial velocity. The energy transferred to the electron is then averaged over a velocity distribution characteristic of the electrons in the initial atomic state. The disadvantage is that the atomic binding is not accounted for dynamically during the collision. This approach, however, has been quite successful in calculations of total cross sections for single and multiple inner-shell ionization.

The SCA was used for most calculations in this paper for three reasons. First, heavy, fast particles having de Broglie wavelengths small compared to atomic dimensions were involved. Second, knowledge of the impact-parameter dependence of the interactions was desired. Third, effects relating to the structure of the atom such as polarization and multiple ionization were required.

In this work two types of refinements of earlier theories concerning Coulomb excitation and ionization of atoms by simple, heavy charged particles are discussed. The first, polarization of the electronic orbitals, concerns the description of collisions of charged particles with a one-electron atom. Deviations from first-order theories are explained by higher order corrections, such as second-order perturbation theory. This is predominately a distant collision effect; i.e., charged particles which pass through the electron cloud make only a small contribution. The second phenomenon, multiple inner-shell ionization of atoms, occurs mainly for close collisions in which the projectile plows through the atom in such a manner as to eject several inner-shell electrons. This many-body effect is thought to occur by either one of two

mechanisms or by both. One is a direct mechanism in which the incident projectile simultaneously ejects two or more electrons. In the other description, a second electron is ejected due to the sudden rearrangement of the atom after an initial electron is ejected.

First-order theories of atomic excitation by particles of charge $Z_1 e$ predict a Z_1^2 dependence of the energy loss and excitation cross section. This is evident in the Born approximation for cross sections [5]:

$$d\sigma_{fi} = 8\pi Z_1^2 \left(\frac{e^2}{\hbar v_1}\right)^2 \frac{2dq}{q^3} |F_{fi}(q)|^2 \qquad [1\text{-}1]$$

and the Bethe-Bloch equation for the stopping power [6]:

$$-\frac{dE}{dx} = \frac{4\pi e^4 Z_1^2 N_0 Z_2}{\mu v_1^2 A} \left[\ln \left(\frac{2\mu v_1^2}{I}\right) - \ln (1 - \beta^2) - \beta^2 - \frac{C}{Z_2}\right]. \qquad [1\text{-}2]$$

In these equations E is the particle energy, x the distance of penetration into the target, μ and $-e$ the electron mass and charge, respectively, v_1 the velocity of the impinging ion, N_0 Avogadro's number, A and Z_2 the atomic weight and number of the target material, I the mean excitation potential of the target material, C/Z_2 the so-called shell corrections, β the ratio of the projectile velocity to the velocity of light, and $\hbar\vec{q}$ the momentum transfer in the collision given by

$$\hbar\vec{q} = \vec{p} - \vec{p}', \qquad [1\text{-}3]$$

where $\vec{p}$ and $\vec{p}'$ are the initial and final momenta of the impinging particle. Also $F_{fi}(q)$ is a form factor given by

$$F_{fi}(q) = \int \psi_f^*(\vec{r})\, e^{i\vec{q}\cdot\vec{r}}\, \psi_i(\vec{r}) d^3r \qquad [1\text{-}4]$$

where ψ_i and ψ_f are the initial and final atomic states, respectively. This Z_1^2 dependence results from the fact that in first order the transition probability due to a perturbation is the square of a matrix element. The matrix element involved in particle-atom collisions is the interaction potential between the particle and the atomic electrons, which is proportional to Z_1. In this work electronic excitations due to collisions between heavy charged particles and atoms will be considered. Deviations from the Z_1^2 law due to the approximations inherent in first-order theory will be discussed.

In recent years advancement of experimental technology has permitted observation of deviations from the Z_1^2 law. One such deviation is the "binding effect", observed for excitation by heavy particles in the energy range, e.g., 0.03-.5 MeV/amu for K-shell ionization of aluminum by light ions [7]. This effect involves the reduction of the electronic excitation cross section due to an increased effective nuclear charge as the heavy ion approaches the atomic nucleus. A second deviation from the Z_1^2 law results from the Coulomb deflection of the incident projectile by the atomic nucleus and is observed, e.g., for ionization of aluminum, for particle energies of 0.02 MeV/amu and lower [7]. In this effect, the excitation cross section becomes dependent upon the projectile charge-to-mass ratio as the slow projectile is deflected from a straight-line path because of interaction with the atomic nucleus. Both the binding effect and the Coulomb-deflection effect have been treated by Basbas, et al. [8].

A third deviation from the Z_1^2 law is the so-called "Z_1^3" effect [3,4]. This is a second-order effect resulting from the polarization

of the atom as the projectile passes by. It tends to increase the interaction cross section for a positive projectile and to decrease the cross section for a negative projectile. This effect will be treated in detail in Chapter 2.

The multiple-ionization effect can be observed by means of satellite lines in x-ray spectra [9]. An x-ray satellite is an x-ray of a different energy, usually higher, than the so-called diagram line. For example a Kα x-ray is produced when a heavy atom with a K-shell vacancy undergoes a radiative transition in filling the vacancy by an L-shell electron. However, if the atom has an additional vacancy in the L shell when the Kα transition occurs, the x ray will be shifted to a slightly higher energy, and is called a KL satellite. The higher energy results because the change in screening due to removal of an L-shell electron shifts the energies of the n=1 and n=2 levels differently. Satellites designated KL^2, KL^3, etc. may be produced if two, three, etc. initial L-shell vacancies, in addition to the K-shell vacancy, are present at the time of K x-ray emission. The energy of the satellite line increases approximately linearly with the number of L-shell vacancies. Vacancies in outer shells also shift the x-ray energies, but by a smaller amount.

In Chapter 3 a discussion of earlier experimental studies and calculations relating to the energy positions and intensities of x-ray satellites is given. A theory is presented which has been used to calculate the multiple-ionization probabilities required in predicting satellite intensities. Section 3.4 is devoted to a discussion of high-resolution measurements of Ti Kα satellite spectra obtained by

bombardment of a titanium target with heavy ions from the tandem Van de Graaff accelerator at the Triangle Universities Nuclear Laboratory. Relative intensities of KL satellite lines as a function of the nuclear charge and energy of the projectile used to excite the spectra are compared with the theory presented in Section 3.3 Shifts in the satellite centroid energies as a function of the projectile nuclear charge are compared with Hartree-Fock calculations in an effort to determine the most probable number of M-shell vacancies present when the Kα transition occurs.

The theories described in this work have served to improve our understanding of the interactions involved in heavy-ion-atom collisions. Toward this end some simplification of atomic wavefunctions was done in order to keep the expressions analytic. At the same time approximations in the treatment of the Coulomb interaction between incident projectile and atomic electrons have been minimized.

Chapter 2

THE Z_1^3 EFFECT

2.1 EXPERIMENTAL OBSERVATION OF THE Z_1^3 EFFECT

In 1963 Barkas et al.[10] measured a range of 708.9 ± 1.5 μm for Σ^- hyperons (v = .143c) in emulsions and deduced a range of 684 ± 5 μm for Σ^+ hyperons at the same energy. The difference was 25 ± 5 μm or about 3.5 percent. They found that the momentum of the Σ^- was incorrectly given by the existing relation [11] between range and momentum. This relation is based upon positive particle ranges. These results implied that the rate of energy loss, or stopping power, for positive ions was greater than that for otherwise identical negative ions at the same velocity. It is true that the Σ^+ and Σ^- particles are not identical, even when the charge difference is ignored. The Σ^+ is less massive by about 0.7 percent than the Σ^-. This means, however, that the range-momentum relation of Ref. 11 should predict a smaller stopping power for the Σ^+ than for the Σ^- of the same momentum, contrary to observation. In other words, the true deviation from the range-momentum relation of Ref. 11 should be greater than that inferred from the $\Sigma^+ - \Sigma^-$ range-difference data. In another experiment Barkas, Osborne, et al. [12] obtained corroboration of the effect from a measurement of range difference between positive and negative pions at $T_\pi \simeq 1.6$ MeV. In 1969 Heckman and Lindstrom [13] made measurements of the grain densities of stopping π^+ and π^- mesons in emulsion. These

measurements showed that, in the velocity interval $.051 < \beta < .178$, the energy loss rates of π^+ mesons exceed those of the π^- meson by amounts of 0 to 60 MeV/cm. These velocities are comparable with those of atomic electrons. The results of this experiment satisfactorily accounted for the previously measured range differences between positive and negative particles. Heckman and Lindstrom also suggested that the apparent differences between the masses of the positive and negative pions [14] might be explained by this effect.

Barkas et al. [10] suggested that the stopping power and range differences were due to deviations from the Born approximation and proposed a charge-dependent correction term. They indicated that such an effect is predicted by a second-order Born approximation stopping power theory. The second Born approximation introduces a term in the stopping power that is proportional to Z_1^3, where Z_1e is the charge of the incident particle. Such a term is of the correct nature to account for the observations. Qualitatively, the effect can be described in terms of a Coulomb attraction or repulsion between the particle and the electrons in the stopping medium. Coulomb attraction of the electrons by a slow positive particle will tend to increase the collision frequency with the electrons, thereby increasing the energy loss rate of the positive particle. Also, a negative particle tends to repel electrons, thereby reducing the electron collision and energy loss rates and increasing the range.

Andersen et al. [15] noted that a charge dependent correction term would also imply that the ratio of the stopping powers for, e.g., alpha particles and deuterons at identical velocities, should deviate from

the factor four predicted by the Bethe formula Eq. (1-2). They measured the stopping powers of aluminum and tantalum for 5-13.5 MeV protons and deuterons and 8-20 MeV ^{3}He and ^{4}He ions. They observed that the ratios of the stopping powers for the doubly-charged ions to those for the singly-charged ions at identical velocities were, indeed, systematically higher than the factor four. The deviation was 2.6 percent in Ta and 1.3 percent in Al at velocities corresponding to proton energies of 2.5 MeV. The relative correction was roughly proportional to E^{-1}, where E is the particle energy. By assuming the deviations to be due to a charge proportional correction to the Bethe equation, Andersen et al. deduced from their measurements a difference in the range of Σ^- and Σ^+ in emulsion. This difference was in agreement with that measured by Barkas et al. [10].

Andersen et al. [15] also examined recently published stopping powers of several elements, as measured by other groups, for alpha particles and protons. They concluded that these data agreed with the effect we are discussing, both in nature and magnitude. They indicated that such an energy-dependent deviation from the Bethe equation would influence the evaluation of the so-called shell correction C/Z_2 from the sum $(\ln I + C/Z_2)_{exp}$. The influence would be in the proper direction to explain the unexpectedly small shell corrections evaluated from the data of Andersen, et al. [16].

The stopping power and range of heavy charged particles penetrating matter receive contributions from the various atomic shells due to excitation and ionization. The major contribution is from the more weakly bound electrons. An effect similar to the deviation from a Z_1^2 law in

the stopping power and range was reported in 1971 by Basbas et al. [7,8], and was verified by Lewis et al. [17]. These groups reported K- and L-shell x-ray yields and ionization cross sections for target atoms of atomic number Z_2 by different energetic particles of atomic number Z_1. The particles included H, D, He, and Li ions having energies of 1-20 MeV/amu.

At particle velocities comparable to or greater than the K-shell electron orbital velocities, ratios of K-shell x-ray yields and cross sections for doubly and triply charged ions to those of singly charged ions showed substantial deviations from the ratios expected on the basis of the theoretically predicted Z_1^2 dependence of the Born approximation and binary encounter descriptions. This effect was attributed to polarization of the electron orbitals by the finite charge of the ionizing particle.

2.2 CALCULATIONS OF THE Z_1^3 CONTRIBUTION

The substantial evidence of deviations from first order theories of stopping power, range, and ionization cross section indicated a necessity for higher order calculations. Second order Born approximation calculations yielding Z_1^3 contributions had been formulated for nuclear Coulomb excitation [18]. These expressions, however, were not readily adaptable to the atomic ionization problem. The first quantitative estimate of the Z_1^3 contribution to the K-shell ionization cross section was proposed by Basbas et al. [8]. They used a simple classical model to estimate the distortion of the K-shell orbits in the field of a passing positive particle. The distortion shortens the effective

interaction distance and thus increases the interaction strength between particle and electron from Z_1 to $Z_1(1-\delta/a_k)^{-1}$, where the ratio of the distortion δ to the K-shell radius a_k, is proportional to Z_1/Z_2. Expansion of this expression in powers of Z_1/Z_2 for $Z_1 \ll Z_2$ gives an additive Z_1^3 contribution to the ionization cross section.

This classical distortion model, however, constituted an ex post facto correction to first order theory. A basic derivation of the effect from first principles was desirable. Such a derivation was published shortly thereafter by Ashley et al. [3]. They made a classical calculation of the Z_1^3 contribution to the energy loss (stopping power), using an isotropic harmonic oscillator as a model for an electron bound in an atom. An impulse approximation, the classical equivalent of the second Born approximation, was used. The resulting Z_1^3 dependent expression was evaluated for a statistical model of the target atoms in the Lenz-Jensen approximation for the electron density distribution $\rho(r)$. Fair agreement of the theory with an estimate of the stopping power derived from the π^+ and π^- data of Heckman and Lindstrom was obtained.

This chapter treats the same problem but gives a fully quantal rather than classical account of the "atom", i.e., the isotropic harmonic oscillator. Since the incident charged particle is described by impact parameter methods, the present calculation is appropriately characterized as semiclassical. Like its predecessor [3], this calculation deals only with the so-called distant collisions, corresponding to large impact parameters and permitting a multipole expansion in inverse powers

of the projectile-target distance. Both calculations involve an exact evaluation of the dipole (E1) contribution to the energy loss and a perturbation treatment of the quadrupole (E2) contribution. All higher multipole terms are neglected.

Section 2.3 provides the theoretical formalism leading to an expression for the energy loss which is identical with the classical result, but the same methods also permit the evaluation of excitation probabilities and inelastic collision cross sections, which have no place in a wholly classical approach. The general formulas are specialized in Section 2.4 to the particular case of an incident charged particle moving uniformly on a straight-line trajectory. A discussion of the model and its possible extension concludes this chapter (Section 2.5).

2.3 GENERAL THEORY

The Coulomb interaction between a classical particle of charge Z_1e at position $\vec{R}(t)$ with coordinates $X(t)$, $Y(t)$, $Z(t)$, and an electron located at position $\vec{r}(x,y,z)$, measured from the atomic nucleus as the origin, is given by

$$V(t) = -\frac{Z_1e^2}{|\vec{R}(t)-\vec{r}|} = -Z_1e^2\{\frac{1}{R(t)} + \frac{\vec{R}(t)\cdot\vec{r}}{[R(t)]^3}$$

$$+ \tfrac{1}{2}\,[\frac{3(\vec{R}(t)\cdot\vec{r})^2}{[R(t)]^5} - \frac{r^2}{[R(t)]^3}] + O(\frac{r^3}{R^4})\} \qquad (2.3\text{-}1)$$

for $R(t)>>r$. The monopole, dipole, and quadrupole terms are of order $\frac{1}{R}$, $\frac{r}{R^2}$, $\frac{r^2}{R^3}$, respectively.

Assuming that the charged particle remains outside the "atom" during the course of its motion, the dipole potential may be regarded as

giving rise to a spatially uniform force which varies in time in a specified manner. The Hamiltonian of the system is conveniently expressed as the sum

$$H = H_1(t) + V_2(t) \tag{2.3-2}$$

of an "unperturbed" part,

$$H_1(t) = H_o + V_1(t) = \frac{p_x^2 + p_y^2 + p_z^2}{2\mu} + \frac{1}{2}\mu\omega^2(x^2 + y^2 + z^2)$$

$$- \frac{Z_1 e^2}{[R(t)]^3}[X(t)x + Y(t)y + Z(t)z] \tag{2.3-3}$$

and a "perturbation",

$$V_2(t) = -\frac{Z_1 e^2}{2}\left\{\frac{3[\vec{R}(t)\cdot\vec{r}]^2}{[R(t)]^5} - \frac{r^2}{[R(t)]^3}\right\} \tag{2.3-4}$$

The monopole term has been omitted from the Hamiltonian, since it does not affect the transition probabilities as long as $R(t) \gg r$ is valid for all t and all pertinent values of r. The Hamiltonian $H_1(t)$ is that of a forced isotropic harmonic oscillator. The equation of motion of such an unperturbed time-dependent quantum system may be solved exactly by separation of variables in the Cartesian coordinates $x = x_1$, $y = x_2$, $z = x_3$.

We introduce raising and lowering operators [19]

$$a_j = \left(\frac{\mu\omega}{2\hbar}\right)^{\frac{1}{2}}\left(x_j + i\frac{p_j}{\mu\omega}\right) \text{ and}$$

$$a_j^{\dagger} = \left(\frac{\mu\omega}{2\hbar}\right)^{\frac{1}{2}}\left(x_j - i\frac{p_j}{\mu\omega}\right), \tag{2.3-5}$$

for the three independent linear oscillators. These satisfy the commutation relations

$$a_j \, a_k^{\dagger} - a_k^{\dagger} \, a_j = \delta_{jk} \tag{2.3-6}$$

The Hamiltonian operator (2.3-3) may be compactly expressed as

$$H_1(t) = H_o + \vec{f}(t)\cdot\vec{a} + \vec{f}^{*}(t)\cdot\vec{a}^{\dagger} \tag{2.3-7}$$

with

$$H_o = \hbar\omega(\vec{a}^{\dagger}\cdot\vec{a} + \frac{3}{2}), \tag{2.3-8}$$

and

$$\vec{f}(t) = -\frac{Z_1 e^2}{[R(t)]^3}\left(\frac{\hbar}{2\mu\omega}\right)^{\frac{1}{2}} \vec{R}(t) \tag{2.3-9}$$

The unitary time development operator in the Schrödinger picture corresponding to the Hamiltonian (2.3-7) and accounting for the evolution of the system from time t_1 to time t_2 is [20]

$$\begin{aligned} T(t_2, t_1) = {} & \exp[i\phi(t_2, t_1)] \exp[-i\omega\vec{a}^{\dagger}\cdot\vec{a}t_2] \\ & \times \exp[-i\vec{g}(\omega;t_2,t_1)\cdot\vec{a} - i\vec{g}^{*}(\omega;t_2,t_1)\cdot\vec{a}^{\dagger}]\exp(i\omega\vec{a}^{\dagger}\cdot\vec{a}t_1) \end{aligned} \tag{2.3-10}$$

where

$$\vec{g}(\omega;\, t_2,\, t_1) = \frac{1}{\hbar}\int_{t_1}^{t_2} e^{-i\omega s}\vec{f}(s)ds, \tag{2.3-11}$$

and $\phi(t_2, t_1)$ is a real phase function.

The perturbation $V_2(t)$ modifies the time development of the system. To first order in the perturbation, the state develops from $\psi(t_1)$ to $\psi(t_2)$ according to the formula

$$\psi(t_2) = [T(t_2, t_1) - \frac{i}{\hbar}\int_{t_1}^{t_2} T(t_2, t)V_2(t)T(t, t_1)dt]\psi(t_1)$$

$$= T(t_2, t_1)[1 - \frac{i}{\hbar}\int_{t_1}^{t_2} T(t_1, t)V_2(t)T(t, t_1)dt]\psi(t_1). \qquad (2.3\text{-}12)$$

The expectation value of an observable A in the final state is, again to first order in V_2,

$$\langle\psi(t_2)|A|\psi(t_2)\rangle = \langle\psi(t_1)|T(t_1, t_2)AT(t_2, t_1)|\psi(t_1)\rangle \qquad (2.3\text{-}13)$$
$$+ \frac{i}{\hbar}\langle\psi(t_1)|[\int_{t_1}^{t_2} T(t_1, t)V_2(t)T(t, t_1)dt, T(t_1, t_2)AT(t_2, t_1)]\psi(t_1)\rangle.$$

Central to the theory are, thus, operator transforms of the type

$$\bar{V}_2(t, t_1) = T(t_1, t)V_2(t)T(t, t_1) . \qquad (2.3\text{-}14)$$

Since $V_2(t)$ is a quadratic form of the operators a_j and $a_j^\dagger$, it is useful to note that standard operator identities give the results

$$T(t_1, t)a_jT(t, t_1) = a_je^{-i\omega(t-t_1)} - ig_j^*(\omega; t, t_1)e^{-i\omega t} \qquad (2.3\text{-}15)$$

and the conjugate relation

$$T(t_1, t)a_j^\dagger T(t, t_1) = a_j^\dagger e^{i\omega(t-t_1)} + ig_j(\omega; t, t_1)e^{i\omega t} \qquad (2.3\text{-}16)$$

The transform of an operator which can be expressed as a polynomial of the a_j and $a_j^\dagger$ is simply obtained by replacing the lowering and raising operators by their transforms.

As a first application, we see that the energy operator for the free isotropic harmonic oscillator undergoes the transformation

$$T(t_1, t_2)H_o T(t_2, t_1) = H_o + \hbar\omega\vec{g}(\omega; t_2, t_1)\cdot\vec{g}^*(\omega; t_2, t_1)$$
$$+ i\hbar\omega\vec{a}\cdot\vec{g}(\omega; t_2, t_1)e^{i\omega t_1} - i\hbar\omega\vec{a}^\dagger\cdot\vec{g}^*(\omega; t_2, t_1)e^{-i\omega t_1} \tag{2.3-17}$$

The quadrupole perturbation operator $V_2(t)$ may be written in the form

$$V_2(t) = \sum_{j,k=1}^{3} Q_{jk}(t)(a_j^\dagger a_k^\dagger + a_j a_k + 2a_j^\dagger a_k) \tag{2.3-18}$$

where the coefficients $Q_{jk}(t)$ are the elements of a real symmetric matrix:

$$Q_{jk}(t) = Q_{kj}(t) = Q_{jk}^*(t) \tag{2.3-19}$$

with a vanishing trace: $\sum_j Q_{jj}(t) = 0$.

The transform of $V_2(t)$ is then found to be

$$\bar{V}_2(t, t_1) = \sum_{j,k} Q_{jk}(t)\{a_j^\dagger a_k^\dagger e^{2i\omega(t-t_1)} + a_j a_k e^{-2i\omega(t-t_1)} + 2a_j^\dagger a_k$$
$$+ 2i[a_j^\dagger e^{i\omega(t-t_1)} + a_j e^{-i\omega(t-t_1)}][g_k(\omega; t, t_1)e^{i\omega t}$$
$$- g_k^*(\omega; t, t_1)e^{-i\omega t}]\} + F(t, t_1)1 \tag{2.3-20}$$

where $F(t, t_1)$ is a c-number function, whose detailed form is not relevant.

If we wish to calculate the energy transfer and related quantities for the overall collision, we must choose $t_1 \to -\infty$ and $t_2 \to +\infty$ in Eq. (2.3-13). We shall also assume as an initial condition that the oscillator is in the ground state $|0\rangle$ before the collision, i.e., $\psi(-\infty) = |0\rangle$. The expectation value of the oscillator energy is then readily obtained from equations (2.3-14), (2.3-17), and (2.3-20). Only

the linear terms in $\bar{V}_2$ contribute to the expectation value of the commutator, and we find:

$$\langle\psi(+\infty)|H_o|\psi(+\infty)\rangle = \frac{3}{2}\hbar\omega + \hbar\omega|\vec{g}(\omega)|^2$$

$$+ 2i\omega \int_{-\infty}^{+\infty} \sum_{j,k} Q_{jk}(t)[g_j(\omega)e^{i\omega t} + g_j^*(\omega)e^{-i\omega t}]$$

$$\chi\ [g_k(\omega;\ t,\ -\infty)e^{i\omega t} - g_k^*(\omega;\ t,\ -\infty)e^{-i\omega t}]dt \qquad (2.3\text{-}21)$$

where the quantity $\vec{g}(\omega)$ is defined by

$$\vec{g}(\omega) = \vec{g}(\omega;\ +\infty,\ -\infty) = \frac{1}{\hbar}\int_{-\infty}^{+\infty} e^{-i\omega s}\vec{f}(s)ds \qquad (2.3\text{-}22)$$

The evaluation of formula (2.3-21), based on detailed assumptions about the time dependence of the coefficients $Q_{jk}(t)$, will be given in the next section. Before proceeding to these calculations, it is useful to relate the expectation value (2.3-21) of the oscillator energy to the total probability of exciting the oscillator from its ground state.

The probability of finding the oscillator at $t = +\infty$ still in the ground state denoted by $|0\rangle$, if it was initially in the ground state, is given by the expectation value (2.3-13) for the operator

$$A = |0\rangle\langle 0| \qquad (2.3\text{-}23)$$

The operator transform needed is

$$T(t_1,t_2)|0\rangle\langle 0|T(t_2,\ t_1) = \exp[-|\vec{g}(\omega;\ t_2,\ t_1)|^2]\exp[-i\omega\vec{a}^\dagger\cdot\vec{a}t_1]$$

$$\chi\ \exp[-i\vec{g}^*(\omega;\ t_1,\ t_2)\cdot\vec{a}^\dagger]|0\rangle\langle 0|\exp[-i\vec{g}(\omega;t_2,t_1)\cdot\vec{a}]\exp[i\omega\vec{a}^\dagger\cdot\vec{a}t_1] \qquad (2.3\text{-}24)$$

Substituing Eqs. (2.3-20), (2.3-23), and (2.3-24) into Eq. (2.3-13) and noting that

$$\vec{g}(\omega;t_1,t_2) = -\vec{g}(\omega;t_2,t_1) \tag{2.3-25}$$

we arrive, after some simple but lengthy manipulations, at

$$|\langle 0|\psi(+\infty)\rangle|^2 = \exp[-|\vec{g}(\omega)|^2]$$

$$\chi \{1 - \frac{2i}{\hbar}\int_{-\infty}^{+\infty}\sum_{jk} Q_{jk}(t)[g_j(\omega)e^{i\omega t} + g_j^*(\omega)e^{-i\omega t}]$$

$$\chi [g_k(\omega;t,-\infty)e^{i\omega t} - g_k^*(\omega;t,-\infty)\, e^{-i\omega t}]\ dt + \frac{i}{\hbar}\int_{-\infty}^{+\infty}\sum_{jk} Q_{jk}(t)$$

$$\chi [g_j(\omega)g_k(\omega)e^{2i\omega t} - g_j^*(\omega)g_k^*(\omega)e^{-2i\omega t}]dt\} \tag{2.3-26}$$

The probability of finding the oscillator at $t = +\infty$ in the eigenstate $|n_1n_2n_3\rangle$, if it was initially in the ground state, is obtained by letting $A = |n_1n_2n_3\rangle\langle n_1n_2n_3|$ in equation (2.3-13).

If n_1, n_2, n_3 are the Cartesian quantum numbers, corresponding to an energy spectrum

$$E = \hbar\omega(n_1 + n_2 + n_3 + \tfrac{3}{2}) \ , \tag{2.3-27}$$

the excitation probability from the initial state $|000\rangle$ is, in analogy with equation (2.3-26), given by

$$|\langle n_1n_2n_3|\psi(+\infty)\rangle|^2 = \exp[-|\vec{g}(\omega)|^2]$$

$$\chi\{\prod_{\ell=1}^{3}\frac{|g_\ell(\omega)|^{2n_\ell}}{n_\ell!} + \frac{i}{\hbar}\int_{-\infty}^{\infty}dt\sum_{j,k=1}^{3}Q_{jk}[e^{i\omega t}g_j(\omega)g_k(\omega) - e^{-2i\omega t}g_j^*(\omega)g_k^*(\omega)]$$

$$\chi [\prod_{\ell=1}^{3}\frac{|g_\ell(\omega)|^{2n_\ell}}{n_\ell!} - 2\prod_{\ell=1}^{3}\frac{|g_\ell(\omega)|^{2(n_\ell-\delta_{j\ell})}}{(n_\ell-\delta_{j\ell})!} + \prod_{\ell=1}^{3}\frac{|g_\ell(\omega)|^{2(n_\ell-\delta_{j\ell}-\delta_{k\ell})}}{(n_\ell-\delta_{j\ell}-\delta_{k\ell})!}]$$

$$-\frac{2i}{\hbar}\int_{-\infty}^{\infty} dt \sum_{j,k} Q_{jk}[g_j(\omega)e^{i\omega t} + g_j^*(\omega)e^{-i\omega t}][g_k(\omega;t,-\infty)e^{i\omega t} - g_k^*(\omega;t,-\infty)e^{-i\omega t}] \chi \left[\prod_{\ell=1}^{3} \frac{|g_\ell(\omega)|^{2n_\ell}}{n_\ell!} - \prod_{\ell=1}^{3} \frac{|g_\ell(\omega)|^{2(n_\ell - \delta_{j\ell})}}{(n_\ell-\delta_{j\ell})!}\right]\} \quad (2.3\text{-}28)$$

where it is understood that terms having denominators such as $(n_\ell-\delta_{j\ell})!$ are zero if $(n_\ell-\delta_{j\ell})$ is a negative integer.

The second term in expression (2.3-26) arises from the terms which are linear in a and $a^\dagger$ in the expansion of the exponential operators in Eq. (2.3-24). The last term, which originates from the quadratic terms in the expansion of the exponentials, vanishes if

$$\sum_{jk} Q_{jk}(-t)g_j^*(\omega)g_k^*(\omega) = \sum_{jk} Q_{jk}(t)g_j(\omega)g_k(\omega) \quad (2.3\text{-}29)$$

For most applications of interest, this time reversal symmetry condition can be satisfied by an appropriate choice of coordinate axes and time origin. If condition (2.3-29) holds, a remarkably simple relation is established between the total excitation probability and the mean energy transfer. By comparing Eqs. (2.3-26), without the last term, and (2.3-21), we obtain

$$|\langle 0|\psi(+\infty)\rangle|^2 = e^{-\Delta E_o/\hbar\omega}\left[1 - \frac{\Delta E-\Delta E_o}{\hbar\omega}\right] \quad (2.3\text{-}30)$$

where ΔE is the energy transfer:

$$\Delta E = \langle\psi(+\infty)|H_o|\psi(+\infty)\rangle - \frac{3}{2}\hbar\omega \quad (2.3\text{-}31)$$

and ΔE_o is the dipole approximation to ΔE:

$$\Delta E_o = \hbar\omega|\vec{g}(\omega)|^2 \quad (2.3\text{-}32)$$

Obviously, to lowest nonvanishing order, (2.3-30) becomes

$$|\langle 0|\psi(+\infty)\rangle|^2 \simeq 1 - \frac{\Delta E}{\hbar\omega} \quad (2.3\text{-}33)$$

indicating that even when the quadrupole perturbation is included to first order, only transitions to the first excited state are important. Thus, if $|\vec{g}(\omega)|^2 \ll 1$, the transition probability to first order in V_2 is simply computed from the energy transfer given by equation (2.3-21).

2.4 STRAIGHT LINE TRAJECTORY MOTION

We are now prepared to calculate the energy transfer to the isotropic oscillator from a charged particle moving on a prescribed orbit. For simplicity we assume that the particle moves with constant velocity v_1 on a straight line trajectory at an impact parameter b. In conformity with Ref. 3, we choose the coordinate system such that the particle moves in the positive y direction on the line X = - b. Hence,

$$X(t) = -b, \qquad Y(t) = v_1 t, \qquad Z(t) = 0 \tag{2.4-1}$$

and consequently

$$f_1(t) = \frac{Z_1 e^2 b}{[b^2 + (v_1 t)^2]^{3/2}} \left(\frac{\hbar}{2\mu\omega}\right)^{1/2}$$

$$f_2(t) = -\frac{Z_1 e^2 v_1 t}{[b^2 + (v_1 t)^2]^{3/2}} \left(\frac{\hbar}{2\mu\omega}\right)^{1/2} \tag{2.4-2}$$

$$f_3(t) = 0$$

and

$$g_1(\omega) = Z_1 e^2 \frac{2\omega}{\hbar v_1^2} \left(\frac{\hbar}{2\mu\omega}\right)^{1/2} K_1\left(\frac{\omega b}{v_1}\right) \tag{2.4-3}$$

$$g_2(\omega) = iZ_1 e^2 \frac{2\omega}{\hbar v_1^2} \left(\frac{\hbar}{2\mu\omega}\right)^{1/2} K_o\left(\frac{\omega b}{v_1}\right)$$

$$g_3(\omega) = 0 \,.$$

The functions K_o and K_1 are modified Bessel functions. For the quadrupole interactions we obtain from Eq. (2.3-4) the following nonvanishing coefficients for expression (2.3-18):

$$Q_{11} = - Z_1 e^2 \frac{\hbar}{4\mu\omega} \frac{2b^2 - (v_1 t)^2}{[b^2 + (v_1 t)^2]^{5/2}}$$

$$Q_{22} = - Z_1 e^2 \frac{\hbar}{4\mu\omega} \frac{2(v_1 t)^2 - b^2}{[b^2 + (v_1 t)^2]^{5/2}} \qquad (2.4\text{-}4)$$

$$Q_{33} = - Z_1 e^2 \frac{\hbar}{4\mu\omega} \frac{-[b^2 + (v_1 t)^2]}{[b^2 + (v_1 t)^2]^{5/2}}$$

$$Q_{12} = - Z_1 e^2 \frac{\hbar}{4\mu\omega} \frac{-3bv_1 t}{[b^2 + (v_1 t)^2]^{5/2}}$$

Applying these results to Eq. (2.3-21) we obtain

$$\Delta E = (Z_1 e^2)^2 \frac{2\omega^2}{\mu v_1^4} \{[K_o(\tfrac{\omega b}{v_1})]^2 + [K_1(\tfrac{\omega b}{v_1})]^2\}$$

$$+ \frac{2(Z_1 e^2)^3}{\mu^2 v_1^4 b^3} \{- K_1(u) \int_{-\infty}^{+\infty} \frac{dv \cos uv}{(1 + v^2)^{5/2}} [(v^2 - 2)F_1(u,v) - 3vF_2(u,v)]$$

$$+ K_o(u) \int_{-\infty}^{+\infty} \frac{dv \sin uv}{(1 + v^2)^{5/2}} [3vF_1(u,v) - (1 - 2v^2)F_2(u,v)]\} \qquad (2.4\text{-}5)$$

where $u = \frac{\omega b}{v_1}$ and [3]

$$F_1(u,v) = \int_{-\infty}^{v} dy \frac{\sin[u(v-y)]}{(1 + y^2)^{3/2}}$$

$$F_1(u,v) = \int_{-\infty}^{v} dy \frac{y \sin[u(v-y)]}{(1 + y^2)^{3/2}} \qquad (2.4\text{-}6)$$

Remarkably, equation (2.4-5) is in exact agreement with the fully classical result [3]. From equations (2.4-3) and (2.4-4) it is seen that the symmetry condition (2.3-29) is satisfied. It follows that the total excitation probability, according to equation (2.3-33), is to the same order of accuracy

$$1 - |\langle 0|\psi(+\infty)\rangle|^2 = \frac{\Delta E}{\hbar\omega} \qquad (2.4\text{-}7)$$

The underlying reasons for the agreement between the quantal and classical ΔE to this order are discussed in Ref. 4.

Equation (2.4-5) has also been derived [4] in conventional perturbation theory, using the free oscillator (Hamiltonian H_o) as the unperturbed system and the interaction $V_1(t) + V_2(t)$ as the time-dependent perturbation. The calculation was repeated in standard perturbation theory because the method employed in this dissertation is peculiar to the isotropic oscillator and not capable of generalization to other, and more realistic, models of the atom. The customary difficulties associated with second-order perturbation theory stand in the way of performing a reliable calculation of the Z_1^3 term for most systems [21], since such a term arises from the interference of first- and second-order transition amplitudes. However, for the isotropic oscillator considerable simplifications occur due to the effect of strong selection rules, and the calculation becomes manageable and transparent. One may even hope that certain features of such a model calculation survive the generalization to more complex systems, perhaps in the form of sum rules.

2.5 DISCUSSION OF THE PRESENT CALCULATION

The integrals appearing in equation (2.4-5) have been evaluated numerically [22]. The overall role of the "distant" collisions can be estimated from the excitation probability for impact parameter b by integrating from a minimum impact parameter, a, to infinity, thereby defining a total excitation cross section for distant collisions:

$$\sigma_d = 2\pi \int_a^\infty (1 - |\langle 0|\psi(+\infty)\rangle|^2) b \, db \qquad (2.5\text{-}1)$$

If relation (2.3-33) holds, this cross section can be expressed in terms of the contributions of the distant collisions to the stopping power:

$$-\left(\frac{dE}{dx}\right)_d = 2\pi n \int_a^\infty \Delta E \, b \, db = n\hbar\omega\sigma_d \qquad (2.5\text{-}2)$$

where n is the number of target atoms per unit volume.

Since at high impact velocities, transition probabilities, cross sections, and energy losses depend on the parameter $\xi = \frac{a\omega}{v_1}$ only logarithmically, when $\xi << 1$, the choice of the minimum impact parameter does not affect the results of the calculations strongly. At such high velocities, it appears reasonable to suppose that the close collisions, with impact parameter less than a, make comparatively small contributions to the Z_1^3 correction term. Such a behavior is said to be expected, since, at high velocities, close collisions may be regarded as impulsive binary collisions between the incident particle and the atomic electron, whose binding to the nucleus is neglected. The strict Z_1^2 proportionality of the Rutherford scattering cross section, appropriate to such a "binary encounter", is then invoked to suggest that close collisions make negligible contributions to the Z_1^3 corrections [3].

Leaving the close collisions aside, the present semiclassical calculation, like its classical predecessor [3], shows the details of a full second-order perturbation calculation for the distant collisions with an oscillator model of the atom. The relation between the semiclassical and the entirely classical theory has been analyzed [4] by considering the equations of motion in the Heisenberg picture, rather than the Schrödinger picture which was used in this dissertation.

2.6 COMPARISON OF Z_1^3 CONTRIBUTION WITH EXPERIMENT

We now consider the Z_1^3 contribution to the excitation cross section. Equation (2.3-26) defines the probability of finding the atom still in the ground state after the collision. For the case of a straight-line trajectory with impact parameter b, this defines the probability

$$P_o(b) = |\langle 0|\psi(+\infty)\rangle|^2 = P_o^{(1)}(b) + P_o^{(2)}(b) \qquad (2.6\text{-}1)$$

where $P_o^{(1)}(b)$ is the first order contribution and $P_o^{(2)}(b)$ is the second order contribution which contains the Z_1^3 term. The probability for excitation is given by

$$P(b) = 1 - P_o(b). \qquad (2.6\text{-}2)$$

Separating first order and second order terms and integrating over impact parameters, we get

$$\sigma^{(1)}(Z_1) = 2\pi \int_a^\infty [1 - P_o^{(1)}(b)]b\, db \qquad (2.6\text{-}3)$$

and $$\Delta\sigma(Z_1) = 2\pi \int_a^\infty P_o^{(2)}(b) b \, db, \qquad (2.6\text{-}4)$$

which are special cases of Eq. (2.5-1). Here $\sigma^{(1)}$ is the first order excitation probability and $\Delta\sigma(Z_1)$ is the contribution to $\sigma(Z_1)$ due to the second order expression. For two particles of charge $Z_1 e$ and $Z_1' e$ we calculate the ratio

$$R \equiv \frac{\sigma(Z_1')}{Z_1'^2 \sigma(Z_1)} \approx \frac{\sigma^{(1)}(Z_1') + \Delta\sigma(Z_1')}{Z_1'^2 \sigma^{(1)}(Z_1)} . \qquad (2.6\text{-}5)$$

This quantity is compared with related experimental cross section ratios taken from the work of Basbas, et al. [8] in Fig. 2. The expression for R was obtained by numerically integrating Eqs. (2.6-3) and (2.6-4) using Eqs. (2.3-22), (2.3-26), (2.4-3) and (2.4-4).

From Fig. 2 it can be seen that the calculation described in this section does roughly reproduce the observed deviation of the K-shell ionization cross section from a Z_1^2 dependence. To obtain the theoretical curves, the parameter $\hbar\omega$ was chosen to be one-half the K-shell binding energy of a hydrogenic atom. The success that Ashley et al. [3] had in extending the energy-loss calculation by means of an oscillator-strength distribution function suggests that a similar approach for our cross section might improve agreement with experiment.

The decrease in the experimental curves at lower energies is due to an effect not included in the polarization calculation of this section. At these low velocities, the increased binding effect [7] dominates over the polarization effect, thereby reducing the extent of the deviation from a Z_1^2 dependence.

Chapter 3

X-RAY SATELLITE LINES AND MULTIPLE IONIZATION THEORY

3.1 HISTORY OF X-RAY SATELLITE OBSERVATIONS

Weak x-ray satellites were first discovered by Siegbahn and Stenstrom [23,24] in the K-emission spectra of elements from Na (11) to Zn (30). M satellites were first reported by Stenstrom [25] in 1918, and L satellites by Coster [26] in 1922. In 1921 Wentzel [27] proposed an explanation for the satellites based on single electron transitions in atoms having multiple inner-shell vacancies. During the years between 1916 and 1942 much work was done on measuring and classifying the x-ray satellite lines [28]. These earlier studies involved either electron excitation or x-ray fluorescence to produce the satellite lines. In electron excitation the target is bombarded under vacuum by a beam of electrons accelerated to a high energy by an electrostatic potential. X-ray fluorescence refers to bombardment of the target by an intense beam of x rays from an x-ray tube. The tube usually produces x rays having a range of energies. The target atom, then, selectively absorbs those x rays having just the right energy to induce an excitation or ionization. Measurements were made by means of high-resolution single- and double-crystal spectrometers. More recent high-resolution studies of x-ray satellites produced by fluorescence and electron impact include those of Deslattes [29].

In 1969 x-ray satellites were re-discovered [30] as energy shifts and broadening of lines in spectra induced by heavy-ion bombardment and observed by medium-resolution solid state detectors. Other measurements [31] verified the shifts. In an attempt to resolve the satellite lines, Bragg crystal spectrometers were installed [32,33] on the beam lines of accelerators. This permitted high resolution observation of x rays due to high energy, heavy-ion bombardment of targets. The broad, shifted peaks were resolved into several separate peaks by these spectrometers. These peaks were identified by means of Hartree-Fock-Slater calculations as satellites of the K x-ray line due to one or more L-shell vacancies when the K transition occurred. Der et al. [34] made direct high-resolution measurements of soft L x rays produced by bombardment of Cu, Zn, and Ni targets with 8-20 MeV oxygen ions. The results substantiated the interpretations of the K x-ray spectra. It was discovered that the satellite structure was greatly enhanced in the heavy-ion induced x rays, and new satellite lines were observed [32]. Following this discovery there was a strong resurgence [35-48] of interest in heavy-ion-induced x-ray spectra. This interest was encouraged by two factors. One was recent improvements in the technology of heavy-ion acceleration. A second factor was the recognition that the enhanced satellite spectra provide a greatly improved probe for studying multiple-ionization mechanisms and for studying in detail the structure of multiply-ionized systems. For example, the study of multiple ionization cross sections may provide information about electron-electron correlation effects [49] in the target. Also, the decay of multiply-excited or ionized states produces rich structure [49] in the x-ray and Auger [50]

spectra. These features can, in some cases, be sensitive to the molecular or solid state environment [45,51-54] of the atom in which the primary ionization occurs. Hence, they may provide information about this environment.

3.2 THEORY OF X-RAY SATELLITE INTENSITIES

Earlier conclusions with respect to the origin of x-ray satellites were, to a large extent, based upon calculations of the energy positions of the satellites [52, 55-57]. Calculations of intensities of satellite lines have apparently been more difficult to make. Such intensity calculations can be divided into two parts. One is the production of multiply-ionized states of the atom. The second is the decay process which may or may not produce x rays. In 1927 Druyvesteyn [58] gave a rather naive semi-classical treatment of the theory of single and double ionization by electron impact. This treatment roughly reproduced the relative intensities of the satellites and the decrease of the first satellite intensity relative to the diagram line with increasing atomic number. In 1935 Bloch [59] made some calculations, using the sudden approximation, of intensities predicted by the double-jump theory, which had been proposed by F. K. Richtmyer [60] in 1928. In this theory a satellite is the combined effect of two simultaneous electron transitions, one occuring in the inner shells and the other in the outer, valence shells. This theory as treated by Bloch was partly successful since it agreed with some satellite intensities. It was discredited shortly after Coster-Kronig transitions were discovered [61] and were shown to explain certain features of L satellite spectra resulting from

x-ray fluorescence. In 1936 R. D. Richtmyer [62] made calculations based on the Born approximation of the effective cross sections for KL ionization (simultaneous ejection of a K-shell and an L-shell electron) of an atom due to electron excitation. His results agree extremely well with observed relative intensities of the KL satellite for targets in the range Z=22 to Z=38. The results are in slight disagreement for Z<22 and disagree sharply for Z>38. In 1964 Sachenko and Demekhin [54] proposed a single mechanism based on the sudden approximation to explain multiple ionization by both electron and photon excitation of the atom. They appear to have been the first to use the binomial statistical distribution to relate multiple-ionization probabilities to single ionization probabilities. In 1967 Åberg [52] published a general theory, also formulated in terms of the sudden approximation, with regard to x-ray excitation by which he derived KL and KM satellite intensities. His calculations of satellite intensities displayed reasonable agreement with experimental intensities obtained from measurements by Deslattes [29].

Calculations of intensities of satellites due to heavy-ion bombardment have been based upon Coulomb-excitation theories. In 1972 Saltmarsh [39] et al. reported that energy shifts of K_α and K_β x-ray lines and K_α/K_β intensity ratios obtained by Si(Li) detectors showed a projectile-energy dependence similar to that predicted for the L-shell ionization cross section. This suggested to them that these phenomena could be explained by existing Coulomb-excitation theories. Subsequently Hansteen and Mosebekk [63] have used the binomial statistical distribution to relate multiple-ionization probabilities to the single-ionization probabilities. They calculated single ionization probabilities

using the semiclassical approximation (SCA) [61]. McGuire and Richard [64], and Hansen [65] have made similar calculations based on the binary-encounter approximation (BEA).

In Section 3.3 we present a theory of multiple ionization similar to that used by Hansteen and Mosebekk, McGuire and Richard, and Hansen. Different atomic wavefunctions are used to simplify the calculations. Also, effects due to energy loss of the projectile and self-absorption of x rays in the target [5] are incorporated directly into the theory. In Section 3.4 we present high-resolution measurements of titanium K_α x-ray spectra [47,66] produced by bombardment of a thick titanium target with the heavy ions listed in Table (3.4-1). The satellite intensities are compared with the theory developed in Section 3.3 In Section 3.5 we discuss possible reasons for differences between experimental and theoretical satellite intensities. The most probable number of M-shell vacancies is deduced from Hartree-Fock energy calculations. Finally, possible mechanisms for the production of M-shell vacancies are examined.

3.3 THE PRESENT CALCULATION OF INTENSITIES

The formulation for describing multiple ionization is substantially that proposed by Hansteen and Mosebekk [63], McGuire and Richard [64], and Hansen [65]. The semiclassical impact-parameter treatment is used to describe the ion-atom collision [67,68], but the atomic wavefunctions are simplified to make evaluation easier. The projectile is assumed to move on a straight line trajectory with impact parameter b. This is a special case of the curved trajectory illustrated in Fig. 1. It is

assumed that the two K-shell electrons and the 8 L-shell electrons all move independently of each other and that they are removed independently. Let $P_K(E,b)$ represent the probability for removing one of the K-shell electrons by Coulomb ionization induced by a projectile with energy E and impact parameter b. We further assume that the probability for removing any one of the L-shell electrons is independent of the subshell or substate occupied and is equal to $P_L(E,b)$. The probability, then, corresponding to a fixed impact parameter b, of removing simultaneously one K-shell and n L-shell electrons is given by [65]

$$P_{K,nl}(E,b) = 2P_K(E,b)[1 - P_K(E,b)]\binom{8}{n}[P_L(E,b)]^n[1-P_L(E,b)]^{8-n} \qquad (3.3\text{-}1)$$

where $\binom{8}{n}$ is a binomial coefficient. The corresponding cross section is given by

$$\sigma_{K,nl}(E) = 2\pi \int_0^\infty P_{K,nL}(E,b)b\, db. \qquad (3.3\text{-}2)$$

It was suggested by Saltmarsh et al. [39] that the observed multiple K- and L-shell Coulomb ionizations might originate from impact parameters deep inside the L electron shell. This was confirmed by calculations of Hansteen and Mosebekk [63]. They show that $P_L(E,b)$ is essentially constant in the region over which $P_K(E,b)$ is non-negligible, and furthermore, that $P_K(E,b)$ is small compared to unity. It is, therefore, a good approximation to replace $(1-P_K)$ by unity, and to approximate $P_L(E,b)$ by $P_L(E,0)$. We will drop the zero and denote the zero-impact-parameter excitation probability for an L-shell electron by $P_L(E) \equiv P_L(E,0)$. The multiple-excitation cross section reduces to

$$\sigma_{K,nL}(E) = 2\sigma_K(E) \binom{8}{n} [P_L(E)]^n [1-P_L(E)]^{8-n}, \qquad (3.3\text{-}3)$$

where

$$\sigma_K(E) = 2\pi \int_0^\infty P_K(E,b)\, bdb \qquad (3.3\text{-}4)$$

is the cross section for removing a K-shell electron.

In the present calculation $\sigma_K(E)$ and $P_L(E)$ were determined by approximating initial and final atomic states by three dimensional, isotropic harmonic oscillator wavefunctions. This drastic approximation was made for several reasons. First, harmonic oscillator wavefunctions are separable in cylindrical coordinates. This enables one to simplify the calculations by exploiting the cylindrical symmetry of the head-on collision problem, b = 0. Second, the calculations were meant to be a preliminary investigation of the projectile Z and energy dependence of multiple excitations. It was felt that a simplified Coulomb-excitation model which might yield the gross properties of the multiple ionization phenomenon, would be more instructive at this point than would a more cumbersome exact model. To obtain $\sigma_K(E)$ and $P_L(E)$ at the many energy values needed to perform the numerical integration involved in thick target corrections could be time-consuming and expensive if accurate atomic wavefunctions were used. Third, it was desirable to have expressions which were available and simple to evaluate, and which would generate $\sigma_K(E)$ and $P_L(E)$ from first principles. Fourth, it was known from earlier work [69,70] that the wavefunctions describing the ground state and the first few excited states of a hydrogenic atom can be moderately well approximated by a linear combination of one to four harmonic oscillator states, providing the oscillator energy-level separation

$\hbar\omega$ is properly related to the binding energy of the atomic state in question. Roughly speaking an oscillator level spacing equal to one-half the binding energy gives good results. Fifth, the selection rules for matrix elements using harmonic oscillator wavefunctions are, in general, much stronger than those for Coulomb wavefunctions. Sixth, analytic harmonic-oscillator expressions of the type desired were available [69] and were simple and easy to evaluate by computer.

The idea of treating the atom as a collection of oscillators is not new. In the radiation theory of the old quantum mechanics, electrons were pictured as classical oscillating dipole emitters or resonant absorbers of radiation. The discrete spectral lines characteristic of an atom were each associated with an oscillator of a particular frequency, and each oscillator was weighted according to an oscillator strength. These oscillator strengths satisfy simple sum rules. It was, then, only natural to extend the idea of oscillator strengths to excitation by means other than photons by defining generalized oscillator strengths and to speculate that the calculations presented in this paper, using harmonic oscillator wavefunctions, might be related to more general atomic descriptions by sum rules.

The K-shell ionization cross section $\sigma_K(E)$ was calculated by the plane wave Born approximation [5] (PWBA) using three-dimensional, isotropic, harmonic oscillator wavefunctions to describe both the initial and final electronic states. Since the harmonic oscillator has no continuum states, this is a rather drastic approximation, but seems to work well for our problem. The differential cross section in this approximation for excitation from an initial state $|i\rangle$ to a final state $|f\rangle$ is given by

$$\frac{d\sigma}{d\Omega} = \frac{4M^2 Z_1^2 e^4}{\hbar^4} \frac{|F_{fi}(q)|^2}{q^4} \tag{3.3-5}$$

with

$$\vec{q} = \vec{k}_i - \vec{k}_f. \tag{3.3-6}$$

Here $F_{fi}(q)$ is defined by Eq. (1-4); $\vec{k}_i$ and $\vec{k}_f$ are the initial and final wavevectors, respectively, of the incident projectile; $\hbar\vec{q}$ is the momentum transferred to the electron in the collision; M and $Z_1 e$ are the reduced mass and charge of the projectile; e is the electronic charge; and ψ_i and ψ_f are the initial and final atomic wavefunctions. We separate the wavefunctions into products of a radial function $R_{n\ell}(r)$ and a spherical harmonic $Y_{\ell m}(\theta,\phi)$

$$\psi_{n\ell m}(\vec{r}) = \frac{R_{n\ell}(r)}{r} Y_{\ell m}(\theta,\phi) \tag{3.3-7}$$

where

$$R_{n\ell}(r) = \frac{[2(n!)\beta^{\frac{1}{2}}]^{\frac{1}{2}}}{[\Gamma(n+\ell+\frac{3}{2})]^{3/2}} \beta^{\frac{\ell}{2}+\frac{3}{4}} r^{\ell+1} e^{-\frac{\beta r^2}{2}} L_n^{\ell+\frac{1}{2}}(\beta r^2) \tag{3.3-8}$$

is the harmonic oscillator radial wavefunction. Here $L_n^{\ell+\frac{1}{2}}$ is an associated Laguerre polynomial. The parameter β is given by

$$\beta = \frac{\mu\omega}{\hbar} \tag{3.3-9}$$

where $\hbar\omega$ is the harmonic oscillator energy-level separation, and μ is the electronic mass. The energy of our "atom" is given by

$$E_{n\ell} = \hbar\omega(2n + \ell + \tfrac{3}{2}) \tag{3.3-10}$$

with

$$\begin{aligned} n &= 0,1,2,\ldots \\ \ell &= 0,1,2\ldots \\ \text{and } m &= 0,\pm1,\pm2,\ldots,\pm\ell. \end{aligned} \tag{3.3-11}$$

By straightforward methods we derive for excitation from the ground state (000) to the first excited state (01m), summed over m,

$$\sum_{m=-1}^{1} |f(q)|^2 \frac{(MZ_1e^2)^2}{\beta^2\hbar^4} \left(\frac{2\beta}{q^2}\right) e^{-\frac{q^2}{2\beta}} \tag{3.3-12}$$

where

$$f(q) = \frac{2MZ_1e^2}{\hbar^2} \frac{F(q)}{q^2} . \tag{3.3-13}$$

The total cross section is given by

$$\sigma = \int_0^{2\pi} d\phi \frac{1}{2k_ik_f} \int_{k_i-k_f}^{k_i+k_f} \sum_m |f(q)|^2 \, d(q^2) . \tag{3.3-14}$$

For fast, heavy particles this reduces to

$$\sigma \approx \frac{2\pi}{\beta} \frac{Z_1^2e^4}{\hbar^2v^2} E_1 \left(\frac{\hbar\omega}{2\mu v^2}\right) \tag{3.3-15}$$

where

$$E_1(x) = \int_x^{\infty} \frac{e^{-x'}}{x'} dx' \tag{3.3-16}$$

is an exponential integral [72].

It is interesting to note that this expression may also be obtained from an earlier, and quite different, derivation given by J. Wu [68] by summing subshell cross sections. Wu's derivation was formulated in cylindrical coordinates using the SCA. The identical final result of the two different calculations is expected from a general theorem [73] which states that a total cross section derived in a straight-line SCA formulation should be identical to the corresponding Born-approximation cross section, for large energies of the particle.

The head-on collision ("L-shell" ionization) probability $P_L(E)$ was similarly calculated in the SCA for excitation from the first excited

level of a harmonic oscillator to the second excited level. In this approximation the amplitude for excitation from an initial state $|i\rangle$ to a final state $|f\rangle$ by a projectile with charge $Z_1 e$ is given in first order perturbation theory by [19]

$$C_{fi}(+\infty) = -\frac{iZ_1e^2}{\hbar}\langle f|\int_{-\infty}^{\infty}\frac{e^{i\omega_{fi}t}}{|\vec{r}-\vec{R}(t)|}dt\,|i\rangle \qquad (3.3\text{-}17)$$

where

$$\hbar\omega_{fi} = E_f - E_i\ . \qquad (3.3\text{-}18)$$

Here E_i and E_f are, respectively, the energies of the intial and final atomic states. If we describe the head-on collision in cylindrical coordinates with origin at the atomic nucleus and the projectile moving along the z-axis with constant velocity v_1, we get

$$|\vec{r} - \vec{R}(t)|^2 = \rho^2 + (v_1t - z)^2, \qquad (3.3\text{-}19)$$

where ρ and z are two coordinates of the electron. This choice of coordinates was made because of the cylindrical symmetry of the collision. Performing the time integration, we obtain

$$C_{fi} = \frac{2Z_1e^2}{\hbar v_1}\langle f|\exp\frac{-i\omega_{fi}z}{v_1}\ K_o\ (\frac{\omega_{fi}\rho}{v_1})\ |i\rangle, \qquad (3.3\text{-}20)$$

where K_o is a modified Bessel function of the second kind and order zero.

The wavefunction for an electron in a harmonic oscillator potential can be expressed in cylindrical coordinates (ρ,ϕ,z) as [74]

$$\Psi_{kmn}(\rho,\phi,z) = R_k(\rho)\ \Phi_m(\phi)\ Z_n(z) \qquad (3.3\text{-}21)$$

where

$$R_{km}(\rho) = \left[\frac{2\beta^{|m|+1}k!}{(k+|m|)!}\right]^{\frac{1}{2}} \rho^{|m|} e^{-\frac{\beta\rho^2}{2}} L_k^{|m|}(\beta\rho^2) , \qquad (3.3\text{-}22)$$

$$\Phi_m(\phi) = \frac{1}{\sqrt{2\pi}} e^{im\phi} , \qquad (3.3\text{-}23)$$

$$Z_n(z) = \frac{\beta^{\frac{1}{4}}}{(2^n n!\sqrt{\pi})^{\frac{1}{2}}} H_n(\sqrt{\beta}z) e^{-\frac{\beta z^2}{2}} , \qquad (3.3\text{-}24)$$

and H_n is the Hermite polynomial. The energy levels are given by

$$E_{kmn} = (2k + |m| + n + 3/2)\hbar\omega$$

$$k = 0,1,2,\ldots$$

$$m = 0,\pm1,\pm2,\ldots \qquad (3.3\text{-}25)$$

$$n = 0,1,2,\ldots$$

We consider excitation from state (kmn) to state (k'm'n'), and write Eq. (3.3-20) as

$$C_{fi} = \frac{2Z_1e^2}{\hbar v_1} I_\rho I_\phi I_z , \qquad (3.3\text{-}26)$$

where

$$I_\rho = \int_0^\infty K_o\left(\frac{\omega_{fi}\rho}{v_1}\right) R_{k'm'}(\rho) R_{km}(\rho) \rho \, d\rho \qquad (3.3\text{-}27)$$

$$I_z = \int_{-\infty}^{\infty} Z_{n'}(z) Z_n(z) e^{\frac{i\omega_{fi}z}{v_1}} dz \qquad (3.3\text{-}28)$$

and

$$I_\phi = \int_0^{2\pi} \Phi_{m'}^*(\phi)\Phi_m(\phi)d\phi = \delta_{mm'} . \qquad (3.3\text{-}29)$$

After some algebraic manipulation we get

$$I_z = \left[\frac{2^{n'}n!}{2^n n'!}\right]^{\frac{1}{2}} e^{-\frac{a^2}{2\beta}} \left(\frac{ia}{2\sqrt{\beta}}\right)^{n'-n} L_n^{n'-n}\left(\frac{a^2}{2\beta}\right) \qquad (3.3\text{-}30)$$

where

$$a = \frac{\omega_{fi}}{v_1} . \qquad (3.3\text{-}31)$$

The integration of Eq. (3.3-27) is more difficult. We use the integral representation [75]

$$K_o(a\rho) = \frac{1}{2}\int_0^\infty \exp[-\frac{a}{2}(t + \frac{\rho^2}{t})]t^{-1}\,dt \qquad (3.3\text{-}32)$$

and set k=0, since we are interested in excitation from the first excited state only, which we will call the "L-shell". This gives

$$I_\rho(k=0) = \frac{1}{2}\int_0^\infty \frac{t^{|m|}e^{-\frac{at}{2}}}{(t + \frac{a^2}{2\beta})^{|m|+1}}\,dt\ . \qquad (3.3\text{-}33)$$

In Table I we list the sublevels of the "L-shell". Also listed are the accessible final sublevels of the second excited level, the "M-shell", consistent with the requirement m'=m as dictated by Eq. (3.3-29). The probability for transition i → f is given by

$$P_{fi} = |C_{fi}(+\infty)|^2 = \frac{4Z_1^2e^4}{\hbar^2v_1^2}|I_\rho|^2|I_\phi|^2|I_z|^2\ , \qquad (3.3\text{-}34)$$

where we have used Eq. (3.3-26). If we substitute Eqs. (3.3-29), (3.3-30), and (3.3-33) into Eq. (3.3-34) we get for the transitions in Table I:

$$P_1 = A^2\,[4t(1-t)E_1(t)]^2$$

$$P_2 = 8A^2t^2\,[e^{-t} - t\,E_1(t)]^2 \qquad (3.3\text{-}35)$$

and

$$P_3 = 8A^2t^2\,[e^{-t} - (1+t)E_1(t)]^2$$

where

$$t = \frac{\hbar\omega}{4\mu v^2}$$

$$A = \frac{Z_1e^2}{r_o}\frac{1}{\hbar\omega} \qquad (3.3\text{-}36)$$

and

$$r_o = (\frac{\hbar}{\mu\omega})^{\frac{1}{2}}\ .$$

If we assume the three "L-subshells" are equally likely to be populated, we can define an average "L- to M-shell" excitation probability by

$$P_L = 1/3\ (P_1 + P_2) + 2/3\ P_3\ . \qquad (3.3\text{-}37)$$

This expression defines our "L-shell ionization probability" for a head-on collision to be used in Eq. (3.3-3).

As the projectile penetrates the target, it loses energy. Thus excitations are produced by the projectile over a continuous range of energies from the initial energy E down to zero. Also the x rays produced within the target may be absorbed before they can leave the surface. The resultant yield of x rays produced in a thick target is given by integrating over the region of penetration into the target according to the following formula [5]:

$$Y_{K,mL}(R_o) = \frac{n}{4\pi} \int_0^{R_o} \omega_K[E(R)]\ e^{-\mu(R-R_o)}\ \sigma_{K,mL}[E(R)]dR\ . \qquad (3.3\text{-}38)$$

This formula is valid if the incident beam of particles and observed x rays form equal angles with a normal to the face of the target. Here R represents the depth of penetration of the projectile into the target at a given instant, E(R) the projectile energy at this depth, R_o the maximum depth or range of a projectile having initial energy E, and ω_K the K-shell fluorescence yield defined as the fraction of atoms, having an initial K-shell vacancy, which yield a K x ray. For the purpose of this calculation we assume that ω_K is independent of the projectile energy and the degree of multiple ionization. The quantity μ is the mass attenuation coefficient which defines the absorption of the x rays as they emerge from the target. Although μ is usually quite energy dependent, it varies little for Ti Kα x rays over the range of interest, and

will be assumed constant. The quantity n is the number density of target atoms.

If we define the stopping power

$$S(E) = -\frac{dE}{dR} , \tag{3.3-39}$$

we can change variables and write

$$Y_{K,mL}(E) = \frac{n\omega_K}{4\pi} \int_0^E e^{-\mu[R(E')-R_o]} \frac{\sigma_{K,mL}(E')}{S(E')} dE' . \tag{3.3-40}$$

Now, if we define

$$Y_K(E) = \frac{n\omega_K}{4\pi} \int_0^E e^{-\mu[R(E')-R_o]} \frac{2\sigma_K(E')}{S(E')} dE' , \tag{3.3-41}$$

we can calculate satellite fractions $F_m(E)$ as

$$F_m(E) = \frac{Y_{K,mL}(E)}{Y_K(E)} \tag{3.3-42}$$

where m can range from zero to eight in theory. $F_m(E)$ is our theoretical prediction for the ratio of the m-th satellite intensity to the total K x-ray intensity. This expression is graphed in Figs. 7 through 10. The stopping power S(E) and range R(E) were taken from the tables of Northcliffe and Schilling [76] and μ was taken from the tables calculated by Dewey *et al.* [77]. The fluorescence yield ω_K was assumed to be the same for all satellites for the purposes of these illustrative calculations.

It should be understood that this estimation of σ_K and P_L using harmonic oscillator states was done for expediency, rather than for accuracy. While improvements are desirable, such a simplified model as we have presented finds use in calculations which require the multiple

Coulomb-ionization cross sections for many projectiles and targets at many energy values. Such usage, however, should be preceded by a thorough study of the limitations of the model and of the best values of the parameter $\hbar\omega$ to be used in a particular situation.

Improvements which might be incorporated into the model include adjustments of the target electron binding energies to reflect the different average binding for different degrees of ionization and properly accounting for variations in fluorescence yield with the degree of ionization.

3.4 EXPERIMENTAL OBSERVATION OF TITANIUM K X-RAY SATELLITE LINES

Multiple inner-shell ionization of atoms by heavy-ion bombardment produces rich structure in the x-ray [9] and Auger [50] electron satellite spectra. X-ray spectra can, in some cases, be sensitive to the molecular or solid state environment of the emitting atom [45,51-54]. Hence analysis of x-ray satellite spectra due to heavy-ion bombardment provides a probe for studying multiple ionization mechanisms and for studying the structure of multiply-ionized systems and interactions of these systems with their molecular or solid state environment.

In this section we present a study of heavy-ion induced titanium KL^n (single K-shell vacancy, n L-shell vacancies) x-ray satellite spectra. Satellite intensities and energy shifts, believed due mainly to M-shell vacancies, have been measured [47,78] for several projectiles, listed in Table II, having atomic numbers in the range one to eight and energies ranging from one to five MeV/amu.

In our experiments, a thick Ti target was bombarded at an angle of 30° to the normal with microampere beams of the ions listed in Table II.

The ions were accelerated by the FN tandem Van de Graaff accelerator at the Triangle Universities Nuclear Laboratory. The target was also fluoresced by bremsstrahlung x rays arising from a specially designed tube [79] with a gold anode. The tube was operated at 17 keV and 2.5 kW power level. The x-ray fluorescence spectrum was used for wavelength-calibration purposes and to serve as a reference for the centroid-energy-shift measurements of the satellite peaks.

The K x rays emitted by the Ti target as a result of the photon and ion bombardment were energy analyzed by means of a Bragg crystal spectrometer using a silicon crystal in 220 reflection ($2d = 3.84\text{Å}$). Figure 3 shows a schematic drawing of the experimental arrangement. The spectrometer was equipped with a horizontal entrance Soller collimator having an angular divergence of .15°. The x-ray detector was a gas-flow proportional counter with a makrafoil window and a gas mixture of 90% argon and 10% methane at a pressure of 400 Torr. The detector was operated at 1400 V and moved through 2θ while the crystal moved through θ. Spectra were obtained by step-scanning over the desired angular region at angles separated by a preset increment in $\sin\theta$, where θ is the angle between the incident x ray and the Bragg reflection plane of the crystal. The counting time for each angular setting of the spectrometer was controlled by the digital output of a current integrator. This served to minimize effects due to beam fluctuations and to insure that the same amount of charge was collected by the target at each setting.

3.5 COMPARISON OF THEORY WITH EXPERIMENT AND DISCUSSION

In this section satellite intensities are compared with the predictions of a theoretical model [80] described in Section 3.3, for multiple

inner-shell Coulomb ionization. Deficiencies in the theory are discussed, and corrections are suggested to improve agreement between theory and experiment. Energy shifts of the KL^n satellites, which have been reported earlier [33,81,82] are compared with Hartree-Fock x-ray energy calculations for various defect configurations. These comparisons may provide information concerning the number of M-shell vacancies at the time of K x-ray emission. Satellite peak widths may provide further information concerning the number of M-shell vacancies and the multiplet splitting of the incomplete L-shell.

Figure 4 shows typical Ti K_α spectra resulting from bombardment by the various projectiles. The spectra have all been normalized to contain the same number of counts in the characteristic $K_{\alpha_{1,2}}$ peak located near 4509 eV. The high energy satellite peaks, labeled $(2p)^5$, $(2p)^4$, etc., have been attributed to multiple ionization involving a single K- and one or more L-shell electrons. The first satellite originates from a single L-shell vacancy, the second from two L-shell vacancies, etc.

We will use the designation KL^n to refer to one K-shell vacancy and n L-shell vacancies. Three features of the spectra are of particular interest. One is the extremely strong dependence of the satellite intensities upon projectile atomic number Z_1. A second is the dependence of satellite intensities upon projectile energy. The third feature is the shift in the centroid energies of the lines, which increases for increasing Z_1. Also the peaks are increasingly broadened for increasing Z_1 and for increasing degree of L-shell ionization for a given projectile. The dependence of the first and second satellite intensity upon projectile energy can be seen in Fig. 5. The decreasing satellite

intensity for increasing lithium ion energy indicates a decreasing L-shell ionization probability.

The peak intensities and positions were obtained by fitting Gaussian functions to the spectrometer data. Relative peak intensities are summarized in Tables III through VII. Peak centroid energies are summarized in Table VIII. Figure 6 illustrates the projectile energy dependence of the first K_α satellite intensity expressed as a percentage of the total K_α intensity, for excitation by the various projectiles. Figure 7 shows a comparison of experiment and theory for the first satellite relative intensity for excitation by He^{++}. The theory is that developed in Section 3.3 and Ref. 80.

The results of an analysis similar to that of Section 3.3, but using BEA theory is shown for comparison. A similar comparison for excitation by Li^{+++} is shown in Fig. 8 for the first and second satellites. Figure 9 shows the experimental and theoretical relative intensities of the first satellite for excitation by carbon. Note that the intensity increases with increasing projectile energy, in contrast to the decreasing trend for the simpler projectiles. The sharp dip and ensuing rise in the theoretical curve is due to the term $(1-P_L)^7$ in Eq. (3.3-3). As P_L goes through its maximum value of .3, this expression decreases sharply. Thus, this term cannot be ignored as was done by Hansteen and Mosebekk [63]. The second through fifth satellites for C excitation are shown in Fig. 10. Figures 7 through 10 indicate that the theory of Section 3.3 roughly agrees with experiment both in the projectile-energy dependence of the relative intensities and in the dependence upon the degree of L-shell ionization. There are, however, observable

differences between the theoretical and experimental curves, which require explanation.

X-ray satellites result from a two-step process. First, inner-shell and, possibly, outer-shell vacancies must be produced by some mechanism. This leaves the atom in an excited state. The atom will then release its excess energy by ejecting an electron or a photon. The de-excitation process is complicated by a host of possible transitions, many of which may serve to rearrange vacancies. These competing processes must be considered in explaining the intensities of the observed x rays, which represent a small fraction of the many possible emissions.

In discussing the differences between theory and experiment, as evidenced in Figures 7 through 10, we shall consider three major effects. The first is an underestimation of the total satellite intensity. The sum of the theoretical relative intensities at a given energy falls below experiment. This is in constrast to the BEA-binomial theory (Fig.7) which overestimates the first satellite intensity. The second effect is the trend toward better agreement between theory and experiment for higher n (see Figures 8 and 10). The third effect relates to differences in the projectile energy dependences of the theoretical and experimental relative intensities for a given satellite.

The first effect, underestimation of the total satellite intensity, can be attributed to deficiencies in the theory. We can look at two aspects of the theory, the description of the atom and the description of the excitation mechanism. We will first consider effects relating to the properties of our atom. The comparisons of theory with experiment

in Figs. 7 through 10 do not include fluorescence yield corrections. It has been observed that the K-shell fluorescence yield is different for atoms having different numbers of vacancies. Accounting for this fact in the theoretical description would affect the overall theoretical satellite intensity. Also, in our harmonic oscillator "atom" [80] the vacancy production for a given state is attributed entirely to Coulomb excitation from that state to the next higher energy level. Excitations to higher levels are neglected because their probabilities are small. This is quite different from a real atom in which vacancy production can occur with comparable probabilities by excitation to a number of closely spaced bound levels as well as to the continuum. Further, if we choose the harmonic oscillator energy level spacing $\hbar\omega$ to be equal to the binding energy of the level we are considering, as was done for the theoretical curves in figures 7 through 10, the harmonic oscillator radial wavefunction is more compact than more realistic wavefunctions. It decreases more rapidly with increasing radial coordinate r, thus describing a more tightly "bound" electron and implying smaller "ionization" probabilities. A small error is also introduced by the use of an average binding energy U_L for the L_1, L_2 and L_3 subshells.

As far as the collision mechanism is concerned, we are employing the ideas of first order perturbation theory. This perturbation approach, however, describes only part of the overall picture. The validity of its use becomes suspect if the projectile-electron interaction is strong. Strong interactions might occur in the case of highly charged projectiles in close collisions with atoms, especially at the lower projectile velocities. Here, higher orders of perturbation theory

may be appropriate. Also, our calculation fails to include other mechanisms which may be important. Such effects as charge exchange or electron capture by the incident projectile, which become more important for higher-Z_1 ions, might contribute to the higher observed satellite intensities.

The second effect observed in figures 8 and 10, the trend toward better agreement of theory with experiment for larger n, is perhaps fortuitous. It is thought to result from a partial cancellation of deficiencies in the theory, described in the preceding paragraph. Thus, if one could correct the previously described deficiencies, it is argued that theory would overestimate experiment for higher n.

Some possible explanations for this trend are related to excitation effects, and others relate to internal rearrangements and other transitions which may occur before the K x-ray emission. An example of an explanation related to excitation is the failure of the model to include statistical correlation effects between simultaneously ejected electrons. The binomial approximation assumes that the L-shell electrons are removed independently of each other. Certainly, one would expect the probability per electron for ejection of three L-shell electrons, properly corrected for the different number of ways of removing three electrons from eight, to be smaller than that for ejection of one or two, simply on the basis of energy conservation. In fact, Hartree-Fock calculations indicate that the energy required to remove a 2p electron from titanium sequentially increases by about 70 eV for each electron removed. Thus, the sixth 2p electron has a binding energy about 75 percent higher than the first. Hence, the higher n or higher energy

satellites exhibit a reduction in intensity from that predicted on the basis of independent removal of L-shell electrons. For this reason, these intensities agree more closely with a theory such as ours, which is based upon single-electron excitation probabilities that are too small. One could improve the theory by allowing $\hbar\omega$ to be different for each defect configuration in accordance with an average binding energy per electron as predicted by Hartree-Fock calculations. Further improvement could be effected by consideration of L-MM Auger transitions in which a vacancy in the L-shell is filled by an M-shell electron, and a second M-shell electron is ejected. This transition would increase the intensities of the lower n satellites at the expense of the next higher satellites, since each occurrence reduces the number of L-shell vacancies by one. The rate for these transitions probably increases with n due to the presence of an increasing number of L-shell vacancies. One must be careful in making such generalizations, however. Removal of L-shell electrons changes not only the L-M vacancy transition energy, but also the binding energy of the ejected M-shell electron. Thus, better calculations of Auger rates for specific defect configurations are desirable. A comparison of the total L-MX rate for Ti with the K-shell radiative and nonradiative rates, for a single vacancy configuration, indicates that this rearrangement effect might be significant and should be accounted for before comparing theory with experiment. This effect might also contribute to the higher total K satellite intensities if it is large enough.

The third disagreement between theory and experiment, the general energy dependence of the satellite intensities, is probably due entirely

to approximations in our theory. The relevant approximations, used here within the context of perturbation theory, are the use of incorrect wavefunctions, consideration of excitation to only one final state, and failure to consider processes such as charge exchange. Perturbation theory becomes less accurate at lower projectile energies and probably overestimates the excitation probabilities. Further, charge exchange becomes more important at lower energies, especially for the more complex ions. Finally, perturbation theory becomes less valid for the more complex ions which interact strongly with the target.

The centroid energies of the x-ray lines were determined by least-squares fitting of multiple Gaussian curves to the overlapping peaks. The average energy positions of the various satellite peaks for different excitations are summarized in Table VIII. The centroid energy shifts and broadening of the main and KL^n satellite peaks evident in figure 4 and Table IX are presumably due mainly to the existence of M-shell vacancies at the time of the K_α transitions. Other possible contributors are discussed later. A plot of the centroid energies of the main K_α peak and the first two satellites versus the atomic number Z_1 of the projectile is shown in figure 11. The shift is almost linear with Z_1 and indicates an increasing number of M-shell vacancies with increasing Z_1. For excitation by a given projectile, however, no projectile-energy dependence of the energy shifts was noticed. Such shifts have been observed before, but here we report a detailed Z_1-dependence study based on the observed positions of the main line and first satellite in the fluorescence spectrum. All numbers are based on an energy of 4509 eV for the $K_{\alpha_{1,2}}$ fluorescence peak, in agreement with the values quoted by Bearden [83].

To obtain an estimate of the number of M- and higher-shell vacancies that would be consistent with the present observations, we have performed calculations of the x-ray energies for various defect configurations using the Hartree-Fock program of Charlotte-Froese Fischer [84]. The arrows in Fig. 4 indicate calculated energies for initial configurations $1s^1\ 2s^2\ 2p^m\ 3s^2\ 3p^6\ 3d^2\ 4d^2$ with m ranging from one to six, i.e., for the case of no M-shell vacancies. The value of $2p^m$ is indicated by figure 4. Assuming that the characteristic $K_{\alpha_{1,2}}$ peak induced by fluorescence corresponds to the diagram transition with no multiple ionization, we normalized the calculated Hartree-Fock energies to this peak by adding 27 eV. The shift from the arrows of the main and satellite peaks seen in the spectra induced by the heavy ions is due, at least in part, to multiple ionization of the M and N shells. For titanium, there are 12 electrons outside of the L-shell. Hartree-Fock calculations have been performed of x-ray energies of the main and first satellite peaks corresponding to a systematic successive removal of the 12 electrons. It was found that the effect of removing all of the 3d and 4s electrons is on the order of 0.5 eV, which may not be detectable in the present experiment. Removing 3p and 3s electrons, however, has a larger effect. In Fig. 12 we plot the shift in the calculated x-ray energy as a function of the number of 3p and 3s electrons removed for the main and first satellite peaks. The upper boundary of the grey area in each case is drawn through calculated energies obtained by removing all the electrons from the 3p shell, keeping the 3s shell full. The lower boundary of the grey area in each case corresponds to removing two electrons from the 3s shell and the remaining electrons from the 3p shell. The other possibility of removing one electron from the 3s shell and the remaining

electrons from the 3p shell lies between the two boundaries in the grey area. Also shown in Fig. 12 are the experimental shifts from fluorescence observed for the various projectiles. These experimental shifts should correspond to the calculated shifts if fluorescence does not cause multiple ionization of the M-shell and if other effects do not contribute to the observed shifts (these effects are discussed later). It is seen that in addition to a K-shell vacancy, the proton-induced spectra correspond to about one vacancy in the 3s or 3p shell while the oxygen induced spectra correspond to from two to three vacancies in the 3s and 3p shells. Similar conclusions can be drawn from Fig. 12 for the number of 3p and 3s vacancies produced simultaneously with a single K- and single L-shell vacancy. It is seen, however, that the average number of these M-shell vacancies for a given projectile is slightly higher for this latter case. It is important to note that this procedure of comparing experimental and calculated energy shifts is especially useful since the conclusions do not depend on the absolute energies of the diagram lines. A similar analysis of projectile x-ray satellite shifts might clarify some questions concerning the effective charge of an ion as it penetrates a solid.

Our conclusions concerning the number of 3s and 3p vacancies are consistent with the results of Saltmarsh et al. [39]. They also predicted a small probability for 3p vacancies in Fe due to oxygen bombardment. Also, Burch et al. [33] deduced two or three 3p vacancies in Fe due to 30 MeV oxygen bombardment. This small probability is surprising since one would expect a violent collision which removes a K-shell and several L-shell electrons also to remove many M-shell electrons. A

possible explanation is that a highly ionized atom in a solid can capture electrons from the nearby conduction band prior to x-ray emission. It would be interesting to do a similar study for a dilute gaseous target in which there are no free electrons available for capture. Another contributing explanation is that the M-shell Coulomb ionization cross section may be small due to the mismatch of the projectile and electron-orbital velocities. Finally, the observed x rays may be Doppler shifted to lower energies due to recoil of the target atoms, because the x rays are observed at 120° to the direction of the incident projectile motion. It is conceivable that the more massive projectiles might produce larger Doppler shifts.

There are several other observations which support the idea that the satellite energy shifts result from M-shell vacancies. First, the larger energy shifts of a particular satellite peak with increasing projectile Z_1 are consistent with the Z_1 dependence of the Coulomb-ionization cross section for removing M-shell electrons. The Coulomb-excitation mechanism would also explain the lack of projectile energy dependence of the shifts, since the corresponding M-shell cross section is slowly varying in this energy range. The observed increase in satellite intensities with higher projectile Z_1 also suggests a decay mechanism which could produce M-shell vacancies. Higher Z_1 projectiles cause more atoms to have a higher degree of L-shell ionization. Atoms having more L-shell vacancies should sustain a higher rate of L-MM Auger transitions. Each L-MM Auger transition results in an atom having one less L-shell vacancy, but also two more M-shell vacancies.

Another process which produces M-shell vacancies is the L_1-$L_{23}M$ Coster-Kronig transition. Variation of Coster-Kronig rates with

different degrees of L-shell and M-shell ionization might affect the observed M-shell vacancy distribution. Intuitively, one might expect these rates to scale roughly according to the number of electrons and vacancies participating. Thus, higher L-shell ionization would result in an increased probability for one and two L_1-shell vacancies and might tend to increase the L_1-$L_{23}M$ rate. Two other effects, however, would tend to work against this premise. A higher degree of L-shell ionization would leave fewer L_2- and L_3-shell electrons to participate in the Coster-Kronig transitions. Secondly, higher L-shell ionization should be accompanied by higher M-shell ionization. If there are fewer M-shell electrons to participate in L_1-$L_{23}M$ Coster-Kronig transitions, the transition rates should be reduced accordingly.

Larkins has recently shown [85], however, that the L_1-$L_{23}M$ Coster-Kronig transition rates should be more rapidly decreasing functions of the degree of L-shell ionization than our scaling arguments would indicate. In fact, for Ti the Coster-Kronig transitions become energetically forbidden for more than two L-shell vacancies accompanying a K-shell vacancy. The L-shell vacancies increase the binding energy of the M-shell electrons due to decreased screening. This energy becomes higher than the L_1-$L_{23}M$ transition energy, thus making the transitions forbidden.

The preceding paragraphs discussed the increase in the centroid energy shift of a given satellite peak with increasing Z_1. We also notice that for fixed Z_1, the centroid energy shifts increase as we go to higher n, where n is the number of L-shell electrons removed. These shifts are measured from the corresponding fluorescence lines for n = 0 and

n = 1 and from Hartree-Fock calculations, assuming no M-shell vacancies, for higher n. Hartree-Fock calculations indicate that the centroid shifts, corresponding to a given number of M-shell vacancies, should increase as n increases. However, experiment indicates a higher rate of increase of centroid shift with increasing n; this implies that atoms which have a larger number of L-shell electrons removed might also have more M-shell electrons removed. This effect is expected since more violent collisions should be involved in higher L-shell vacancy production, thus also producing more M-shell vacancies.

Another interesting property of the spectra is the line widths of the various satellite peaks as summarized in Table IX. These widths vary from about 10 eV to as much as 37 eV. The extremely wide KL^4 satellites, however, have low intensities. This could result in broadening due to a low peak-to-background ratio and to poor statistics. All peaks, however, are broader than the 6 eV resolution of the spectrometer. The increasing width for a given peak with increasing projectile atomic number Z_1, as seen in Table IX, might be explained as follows. Each KL^n satellite peak is actually a composite of KL^nM^m peaks. Since each M-shell vacancy increases the K x-ray energy $\lesssim$ 1 eV, the spread in M-shell vacancies results in a broadened satellite peak. Higher Z_1 results in a higher degree of M-shell ionization in some atoms, and a resulting wider spread in the number of initial M-shell vacancies. This broadens the satellite peaks.

The increased broadening of the peaks for higher n in a given spectrum can be understood in terms of four effects, each of which may contribute to the broadening. Higher n satellites are produced in more

violent collisions which result in more L- and M-shell vacancies. As explained before, the broader spread in the number of M-shell vacancies results in wider x-ray peaks. The second effect is the multiplet splitting of the incomplete L-shell. This splitting is different for different degrees of L-shell ionization. One would expect a more complex and broader multiplet structure for, e.g., three L-shell vacancies than for two. This is in agreement with the observed trend. A third possible contributor to the increasing widths is Doppler broadening. Heavier, more highly charged projectiles can penetrate closer to the target nucleus and transfer more recoil energy to the target atom. This may result in a wider spread in Doppler-shifted energies of the emitted x rays. Another possible contributor to these increasing widths has been recently pointed out by Watson [86]. For higher satellites two effects are observed. One relates to the different energies of KL(2s) and KL(2p) satellites and the increasing number of ways in which a given number of L-shell vacancies may be distributed over the 2s and 2p subshells. The second effect relates to the energy difference between a K-L_2 and K-L_3 x ray (~ 6 eV if no L- or M-shell vacancies are present). For higher satellites, the relative rates of these two transitions are expected to change due to an increasing complexity in the ways in which electrons may be left in the L_2 and L_3 subshells. To illustrate, three 2p vacancies may consist of two L_2 and one L_3 vacancy, in which case only the K-L_3 x ray may be emitted; or one may have one L_2 and two L_3 vacancies, in which case both K-L_2 and K-L_3 x rays may be emitted; etc. Some of the effects discussed here may be speculative and should be further subjected to quantitative calculations.

To summarize, titanium K_α diagram and satellite x-ray intensities, centroid energies, and peak widths have been studied by high-resolution Bragg crystal spectrometry. Systematic variations in these parameters have been observed as a function of projectile atomic number and of the number of L-shell vacancies. Satellite intensities were also studied as a function of projectile energy. The intensities agree roughly with predictions of a Coulomb-ionization theory modified to account for multiple ionization. Variations in centroid energies and peak widths are consistent with explanations based on M-shell ionization, multiplet splitting of the incomplete L-shell, and variations in the distribution of L-shell vacancies [86] among the three L subshells. Both ionization and decay phenomena may contribute to observed properties of the spectra. More detailed studies of intensities, centroid energies, and peak widths are needed. More sophisticated multiple ionization calculations and better calculations of rearrangement rates would help in interpretation of the spectra.

References

1. Jens Bang and Johannes M. Hansteen, Kgl. Danske Videnskab. Selskab, Mat. - Fys. Medd. 31, no. 13 (1959).
2. M. Gryzinski, Phys. Rev. 138, A336 (1965).
3. J. C. Ashley, R. H. Ritchie, and W. Brandt, Phys. Rev. B5, 2393 (1972).
4. K. W. Hill and E. Merzbacher, Phys. Rev. A9, 156 (1974).
5. E. Merzbacher and H. W. Lewis, Hand. d. Physik 34, 166 (1958).
6. U. Fano, Ann. Rev. Nucl. Sci. 13, 1 (1963).
7. G. Basbas, W. Brandt, and R. Laubert, Phys. Rev. Lett. 34A, 277 (1971).
8. G. Basbas, W. Brandt, R. Laubert, A. Ratkowski, and A. Schwarzschild, Phys. Rev. Lett. 27, 171 (1971).
9. A. R. Knudson, D. J. Nagel, P. G. Burkhalter, and K. L. Dunning, Phys. Rev. Lett. 26, 1149 (1971).
10. W. H. Barkas, J. W. Dyer, and H. H. Heckman, Phys. Rev. Lett. 11, 26 (1963); 11, 138(E) (1963).
11. W. H. Barkas and M. J. Berger, National Academy of Sciences - National Research Council Publication No. 1133, 1964 (unpublished), pp. 103-172; H. H. Heckman, B. L. Perkins, W. G. Simon, F. M. Smith, and W. H. Barkas, Phys. Rev. 117, 544 (1960).
12. W. H. Barkas, W. Z. Osborne, W. G. Simon, and F. M. Smith, CERN Report No. CERN 65-4, 1965 (unpublished), Vol. II.

13. H. H. Heckman and P. J. Lindstrom, Phys. Rev. Lett. 22, 871 (1969).

14. H. W. Barkas, W. Birnbaum, and F. M. Smith, Phys. Rev. Lett. 101, 778 (1956).

15. H. H. Andersen, H. Simonsen, and H. Sørensen, Nucl. Phys. A125, 171 (1969).

16. H. H. Andersen, C. C. Hanke, H. Simonsen, H. Sørensen, and P. Vajda, Phys. Rev. 175, 389 (1968).

17. C. W. Lewis, J. B. Natowitz, and R. L. Watson, Phys. Rev. Lett. 26, 481 (1971).

18. K. Alder, A. Bohr, T. Huus, B. Mottelson, and A. Winther, Rev. Mod. Phys. 28, 432 (1956).

19. E. Merzbacher, Quantum Mechanics (Wiley, New York, 1970), 2nd ed., p. 357.

20. Ibid., p. 365. This is a more general form of equation (15.132).

21. For a brief survey of several approaches to the problem of summation over intermediate states see A. R. Holt and B. L. Moiseiwitsch, J. Phys. B1, 36 (1968).

22. J. C. Ashley, V. E. Anderson, R. H. Ritchie, and W. Brandt, Z_1^3 Effect in the Stopping Power of Matter for Charged Particles: Tables of Functions, NAPS Document No. 02195, to be ordered from ASIS NAPS, c/o Microfiche Publications, 305 E. 46th St., New York, N. Y. 10017, remitting $1.50 for microfiche or $5.00 for photocopy up to 30 pages and $0.15 per each additional page over 30. Estimate 17 pages.

23. M. Siegbahn and W. Stenstrom, Phys. Z. 17, 48 and 318 (1916).

24. The historical discovery of x-ray satellites is reviewed by Anand N. Nigam and Rakesh B. Mathur, page 1698 in U. S. Atomic Energy Commission Report No. CONF - 720404, edited by R. W. Fink, S. T. Manson, J. M. Palms, and P. V. Rao, 1973 (unpublished).

25. W. Stenstrom, Ann. d. Physik 57, 347 (1918).

26. D. Coster, Phil. Mag. 43, 1070 (1922).

27. G. Wentzel, Ann. Phys. (Paris) 66, 437 (1921); Zeits, f. Physik 31, 445 (1925).

28. References to earlier measurements of satellite positions are found in Ref. 24.

29. R. D. Deslattes, Phys. Rev. 133, A 390 (1964).

30. Patrick Richard, I. L. Morgan, T. Furuta, and D. Burch, Phys. Rev. Lett. 23, 1009 (1969).

31. D. Burch and Patrick Richard, Phys. Rev. Lett. 25, 983 (1970); G. A. Bissinger and S. M. Shafroth, Bull. Am. Phys. Soc. 16, 125 (1971).

32. A. R. Knudson, D. J. Nagel, P. G. Burkhalter, and K. L. Dunning, Phys. Rev. Lett. 26, 1149 (1971).

33. D. Burch, Patrick Richard, and R. L. Blake, Phys. Rev. Lett. 26, 1355 (1971).

34. R. C. Der, R. J. Fortner, T. M. Kavanagh, J. M. Khan, and J. D. Garcia, Phys. Rev. Lett. 36A, 239 (1971).

35. A. R. Knudson, D. J. Nagel, and P. G. Burkhalter, Phys. Lett. 42A, 69 (1972).

36. D. G. McCrary and Patrick Richard, Phys. Rev. A5, 1249 (1972).

37. C. F. Moore, M. Senglaub, B. Johnson, and P. Richard, Phys. Lett. 40A, 107 (1972).

38. D. G. McCrary, M. Senglaub, and Patrick Richard, Phys. Rev. A6, 263 (1972).

39. M. J. Saltmarsh, A. van der Woude, and C. A. Ludemann, Phys. Rev. Lett. 2, 329 (1972).

40. C. Fred Moore, David K. Olsen, Bill Hodge, and Patrick Richard, Z. Physik 257, 288 (1972).

41. A. R. Knudson, P. G. Burkhalter, and D. J. Nagel, Bull. Am. Phys. Soc. 18, 559 (1973).

42. David K. Olsen, C. Fred Moore, and Robert L. Kauffman, Bull. Am. Phys. Soc. 18, 559 (1973).

43. B. Budick, A. M. Rushton, L. Skoski, and H. J. Verschell, Bull. Am. Phys. Soc. 18, 560 (1973).

44. R. D. Deslattes, J. W. Cooper, S. M. Shafroth, B. Doyle, R. W. White, and K. W. Hill, Bull. Am. Phys. Soc. 18, 1508 (1973).

45. P. G. Burkhalter, A. R. Knudson, D. J. Nagel, and K. L. Dunning, Phys. Rev. A6, 2093 (1972).

46. R. K. Cacak, S. S. Choe, and F. W. Martin, Bull. Am. Phys. Soc. 18, 1508 (1973).

47. K. W. Hill, B. Doyle, S. M. Shafroth, R. W. White, J. W. Cooper, and R. D. Deslattes, Bull. Am. Phys. Soc. 18, 1509 (1973).

48. P. G. Burkhalter, A. R. Knudson, and D. J. Nagel, Bull. Am. Phys. Soc. 18, 1509 (1973).

49. T. Åberg, page 1509 in Ref. 24.

50. Dennis L. Matthews, B. M. Johnson, J. J. Mackey, L. E. Smith, and C. Fred Moore, Bull. Am. Phys. Soc. 18, 1508 (1973).

51. L. G. Parratt, Rev. Mod. Phys. 31, 616 (1959).

52. Teijo Åberg, Phys. Rev. 156, 35 (1967).

53. J. McWherter, J. E. Bolger, H. H. Wolter, D. K. Olsen, and C.F. Moore, Phys. Lett. 45A, 57 (1973).

54. V. P. Sachenko and V. F. Demekhin, J. Exptl. Theoret. Phys. (U.S.S.R.) 49, 765 (1965) [English transl. Soviet Phys. - JETP 22, 532 (1966)].

55. D. J. Candlin, Proc. Phys. Soc. (London) 68, 322 (1955).

56. Z. Horak, Proc. Phys. Soc. (London) 77, 980 (1961).

57. R. D. Deslattes, Phys. Rev. 133, A399 (1964).

58. M. J. Druyvesteyn, Zeits. f. Physik 43, 707 (1927).

59. F. Bloch, Phys. Rev. 48, 187 (1935).

60. F. K. Richtmyer, Phil. Mag. 6, 64 (1928), and J. Frank. Inst. 208, 325 (1929).

61. D. Coster and R. de L. Kronig, Physica 2, 13 (1935).

62. Robert D. Richtmyer, Phys. Rev. 49, 1 (1936).

63. J. M. Hansteen and O. P. Mosebekk, Phys. Rev. Lett. 29, 1361 (1972).

64. James H. McGuire and Patrick Richard, Phys. Rev. A8, 1374 (1973).

65. J. S. Hansen, Phys. Rev. A8, 822 (1973).

66. D. Madison, K. Hill, B. Doyle, S. M. Shafroth, and R. D. Deslattes (to be published).

67. J. Wu, K. W. Hill, and E. Merzbacher, Bull. Am. Phys. Soc. 18, 662 (1973).

68. J. Wu, thesis (unpublished).

69. K. W. Hill (unpublished).

70. M. Moshinsky and O. Novaro, J.Chem. Phys. 48, 4162 (1968).

71. Philip M. Morse and Herman Feshbach, Methods of Theoretical Physics, Vol. II,p. 1663 (McGraw-Hill Book Co., Inc., New York, 1953).

72. Milton Abramowitz and Irene A. Stegun, editors, Handbook of Mathematical Functions, (National Bureau of Standards Applied Mathematics Series 55, 1968), seventh printing, p. 228.

73. Ref. 1, Appendix I, p. 34.

74. L. C. Pauling and E. B. Wilson, Introduction to Quantum Mechanics, 1st Ed., (McGraw-Hill Book Company, New York, 1935).

75. I. S. Gradshteyn and I. M. Ryzhik, Tables of Integrals, Series, and Products (Academic Press, New York, 1965), fourth edition, p. 959.

76. L. C. Northcliff and R. F. Schilling, Nuclear Data A7, 233 (1970).

77. R. D. Dewey, R. S. Mapes, and T. W. Reynolds, Progress in Nuclear Energy (Pergamon Press, 1969), Series 9, Vol. 9.

78. K. W. Hill, B. L. Doyle, D. H. Madison, S. M. Shafroth, and R. D. Deslattes, to be published.

79. R. D. Deslattes and B. G. Simson, Revs. Sci. Insts. 37, 753 (1966).

80. K. W. Hill, D. H. Madison, E. Merzbacher, and J. Wu (to be published).

81. Joe McWherter, Joe Bolger, C. Fred Moore, and Patrick Richard, Z. Physik, 263, 283 (1973).

82. R. L. Kauffman, F. Hopkins, C. W. Woods, and P. Richard, Phys. Rev. Lett. 31, 621 (1973).

83. J. A. Bearden, Rev. Mod. Phys. 39, 78 (1967).

84. C. Froese Fischer, Comp. Phys. Comm. 4, 107 (1972).

85. F. P. Larkins, J. Phys. B1, 37 (1974).

86. R. L. Watson, private communication.

List of Tables

Table IX Average widths in eV of Ti KL^n x-ray satellite peaks for bombardment by various projectiles. The numbers in parentheses indicate uncertainties.

Table I.

Probability designations and quantum numbers associated with allowed transitions between sublevels of the "L shell" and "M shell" of the isotropic oscillator, as produced by a head-on collision.

PROBABILITY	"L SHELL" k	m	n	"M SHELL" k'	m'	n'
P_1	0	0	1	0	0	2
P_2	0	0	1	1	0	0
P_3	0	± 1	0	0	± 1	1

Table II.

Summary of projectiles and energies presented in this work.

All energies are given in MeV.

Projectile	Energies
H	2.5, 3.5, 4.0, 5.0
^{4}He	4, 6, 9, 12, 18
^{7}Li	10.5, 16.4, 21, 26.25
^{12}C	21, 27, 36, 39, 45,
^{16}O	15, 18, 24, 30, 36, 39, 42.5, 52.3, 60

Table III.

Ratios of Ti KL^n x-ray intensities to total K intensity $\sum_n I(KL^n)$ for incident protons. All energies are in MeV.

Energy	K	KL
2.5	.945	.055
3.5	.956	.044
4.0	.963	.037
6.0	.889	.111

Table IV.

Ratios of Ti KL^n x-ray intensities to total K intensity for incident helium ions. All energies are in MeV.

Energy	K	KL^1	KL^2
4.0	.760	.219	.021
7.5	.795	.186	.018
9.0	.788	.196	.016
11.7	.824	.166	.009
12.0	.842	.158	
13.0	.841	.159	
14.0	.863	.136	
16.0	.865	.135	
18.0	.879	.121	

Table V.

Ratios of Ti KL^n x-ray intensities to total K intensity for incident lithium ions. All energies are in MeV.

Energy	K	KL^1	KL^2
10.5	.499	.403	.098
16.4	.598	.343	.0585
21.0	.622	.331	.0473
26.2	.695	.272	.0355

Table VI.

Ratios of Ti KL^n x-ray intensities to total K intensity for incident carbon projectiles. All energies are in MeV.

Energy	K	KL	KL^2	KL^3	KL^4
21.0	.148	.341	.321	.136	.053
27.1	.161	.352	.317	.138	.032
36.0	.205	.368	.289	.115	.022
39.3	.213	.379	.287	.100	.021
45.0	.254	.388	.259	.086	.013

Table VII.

Ratios of x-ray intensities to total K intensity for incident oxygen projectiles. All energies are in MeV.

Energy	K	KL	KL^2	KL^3	KL^4
15.0	.086	.205	.186		
18.0	.097	.276	.319	.152	.157
24.0	.104	.268	.331	.182	.115
30.0	.102	.264	.328	.171	.135
45.5	.113	.277	.342	.178	.090
52.3	.115	.283	.329	.165	.108
60.0	.115	.286	.314	.184	.101

Table VIII.

Average peak energy positions in eV of Ti KL^n x-ray satellites for bombardment by various projectiles.

Projectile	K	KL	KL^2	KL^3	KL^4
Photon	4509	4533.4			
H	4510.1	4535.4			
He	4511.1	4536.1	4559.8		
Li	4511.9	4536.7	4561.5		
C	4513.7	4538.7	4564.1	4589.9	4616.2
O	4514.6	4541.1	4566.2	4591.6	4614.7

Table IX.

Average widths in eV of Ti KL^n x-ray satellite peaks for bombardment by various projectiles. The numbers in parentheses indicate uncertainties.

Projectile	K	KL	KL^2	KL^3	KL^5
Fluorescence	11.5 (.2)	14.7 (.5)			
H	10.3 (.2)	12.9 (1.5)			
He	10.8 (.2)	12.5 (.3)	14.7 (1.0)		
Li	11.8 (.6)	12.6 (.3)	15.5 (.4)		
C	13.8 (.2)	15.1 (.3)	17.4 (.2)	19.6 (.3)	23.7 (2.1)
O	14.3 (.3)	16.5 (.4)	17.4 (.5)	18.6 (.4)	37.5 (3.0)

Figure Captions

Figure 1 Geometric relations showing projectile Z_1 with impact parameter b passing near target nucleus Z_2 on a Kepler orbit. The projectile reaches the point of closest approach $\vec{R}(o)$ at t = o. The atomic electron is at position $\vec{r}$. The x and x' axes coincide and are perpendicular to the plane of the figure.

Figure 2 Aluminum K-shell ionization ratios. The experimental points from Basbas et al. [8] are the indicated ratios for doubly-to-singly-charged ions (lower curve) and triply-to-single-charged ions (upper curve). The theoretical curves are the corresponding results of the semiclassical calculation of Hill and Merzbacher [4]. The atom was simulated by three-dimensional isotropic harmonic oscillator wavefunctions with $\hbar\omega$ chosen to be approximately one half of the Al K-shell binding energy.

Figure 3 The experimental apparatus for high-resolution energy analysis of target x rays. X rays are produced by bombardment of the target by ion beams or by fluorescence, using the built-in x-ray tube. The x rays are collimated by the entrance Soller collimator, Bragg reflected by the crystal (at center

of spectrometer), and detected by the proportional counter behind the exit collimator.

Figure 4 Ti K_α x-ray spectra. The arrows indicate Hartree-Fock energies for these peaks assuming no vacancies in the M and N shells.

Figure 5 Titanium K_α x-ray spectra for bombardment of a thick Ti target by lithium ions at three different energies. The ordinates are in arbitrary units. The structure noted in the main peak (left) is due to the 6 eV energy difference between the K_{α_1} and K_{α_2} peaks. The decreasing relative intensity of the two satellite peaks with increasing particle energy indicates a decreasing L-shell ionization probability.

Figure 6 Relative intensity of first Ti x-ray satellite peak (KL) expressed as a percentage of the total K_α x-ray intensity. The particles used to produce the x rays are indicated.

Figure 7 Relative intensity of the titanium first K_α x-ray satellite peak (KL) resulting from ionization by helium ions. The dashed line represents a semiclassical approximation (SCA) calculation extended by a binomial statistical distribution to include multiple ionization. The solid curve is a binary encounter approximation (BEA) - binomial distribution calculation done by J. H. McGuire.

Figure 8 Relative intensity of titanium first and second K_α x-ray satellites (KL,KL^2) resulting from bombardment by lithium ions.

Figure 9 Relative intensity of titanium first K_α x-ray satellite resulting from bombardment by carbon ions.

Figure 10 Relative intensity of titanium second, third, and fourth K_α x-ray satellite peaks (KL^2,KL^3, and KL^4) resulting from bombardment by carbon ions.

Figure 11 Experimental Ti KL^n centroid energies as a function of projectile Z for n = 0,1,2.

Figure 12 Shifts in K_α x-ray energies as a function of the number of vacancies in the 3s or 3p shells. The boundaries of the grey area are drawn through calculated HF energy shifts and the horizontal lines are experimental shifts.

Fig. 1

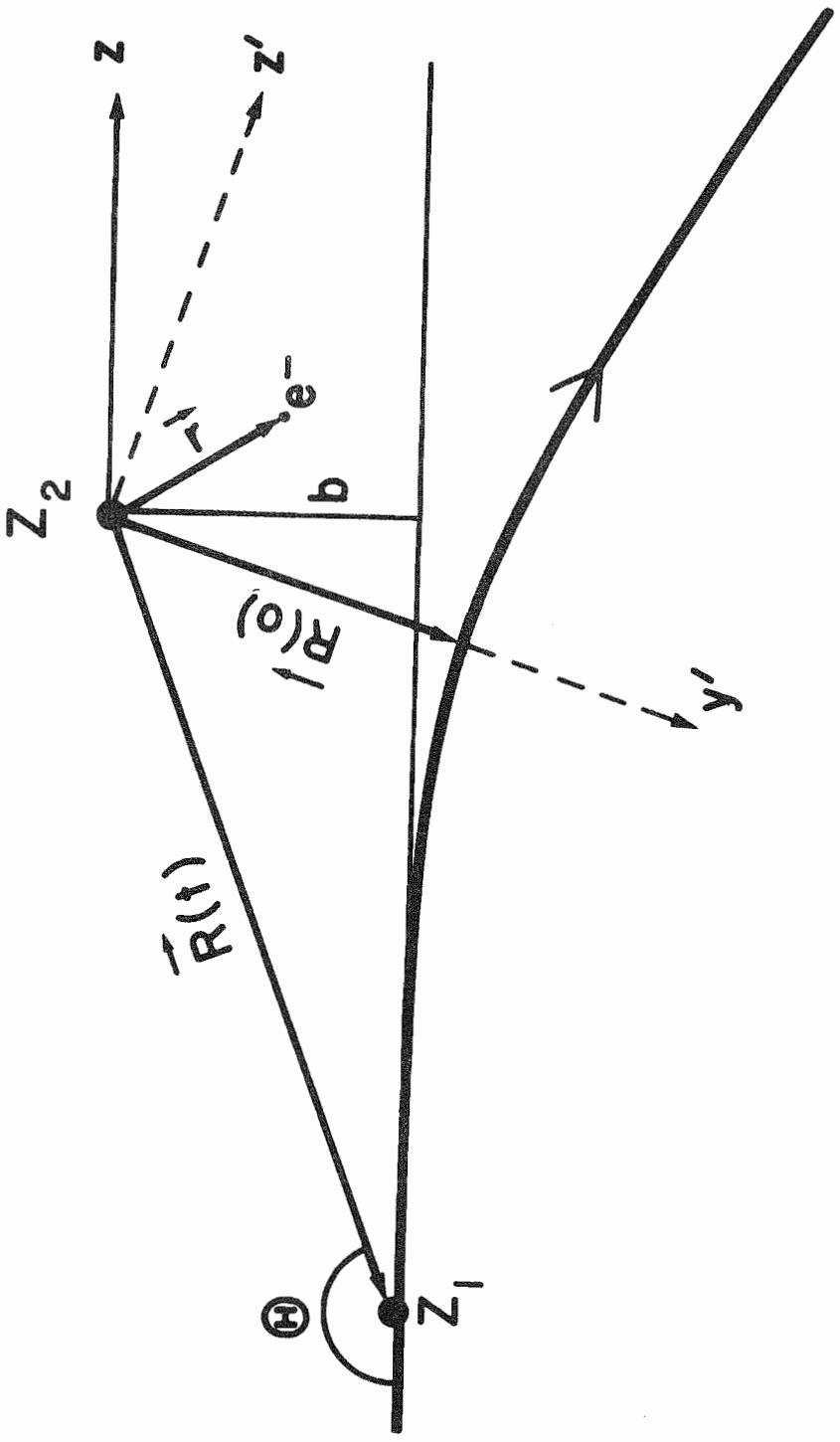

Fig. 2

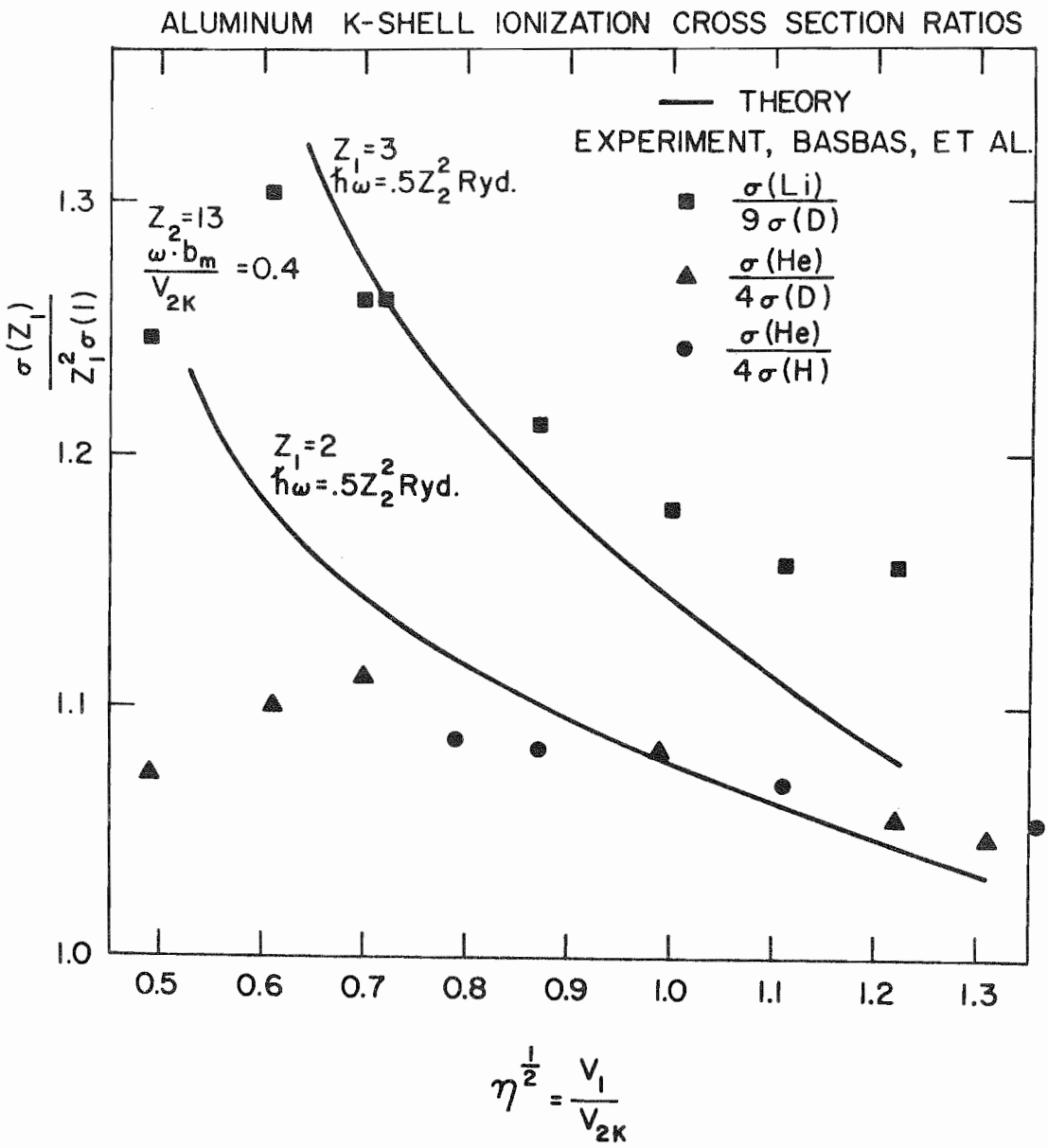
ALUMINUM K-SHELL IONIZATION CROSS SECTION RATIOS
THEORY
EXPERIMENT, BASBAS, ET AL.
σ(Li)/9σ(D)
σ(He)/4σ(D)
σ(He)/4σ(H)
Z1=3
ħω=.5Z2² Ryd.
Z2=13
ω·bm/V2K =0.4
Z1=2
ħω=.5Z2² Ryd.
σ(Z1)/Z1²σ(1)
1.0
1.1
1.2
1.3
0.5
0.6
0.7
0.8
0.9
1.0
1.1
1.2
1.3
η^½ = V1/V2K

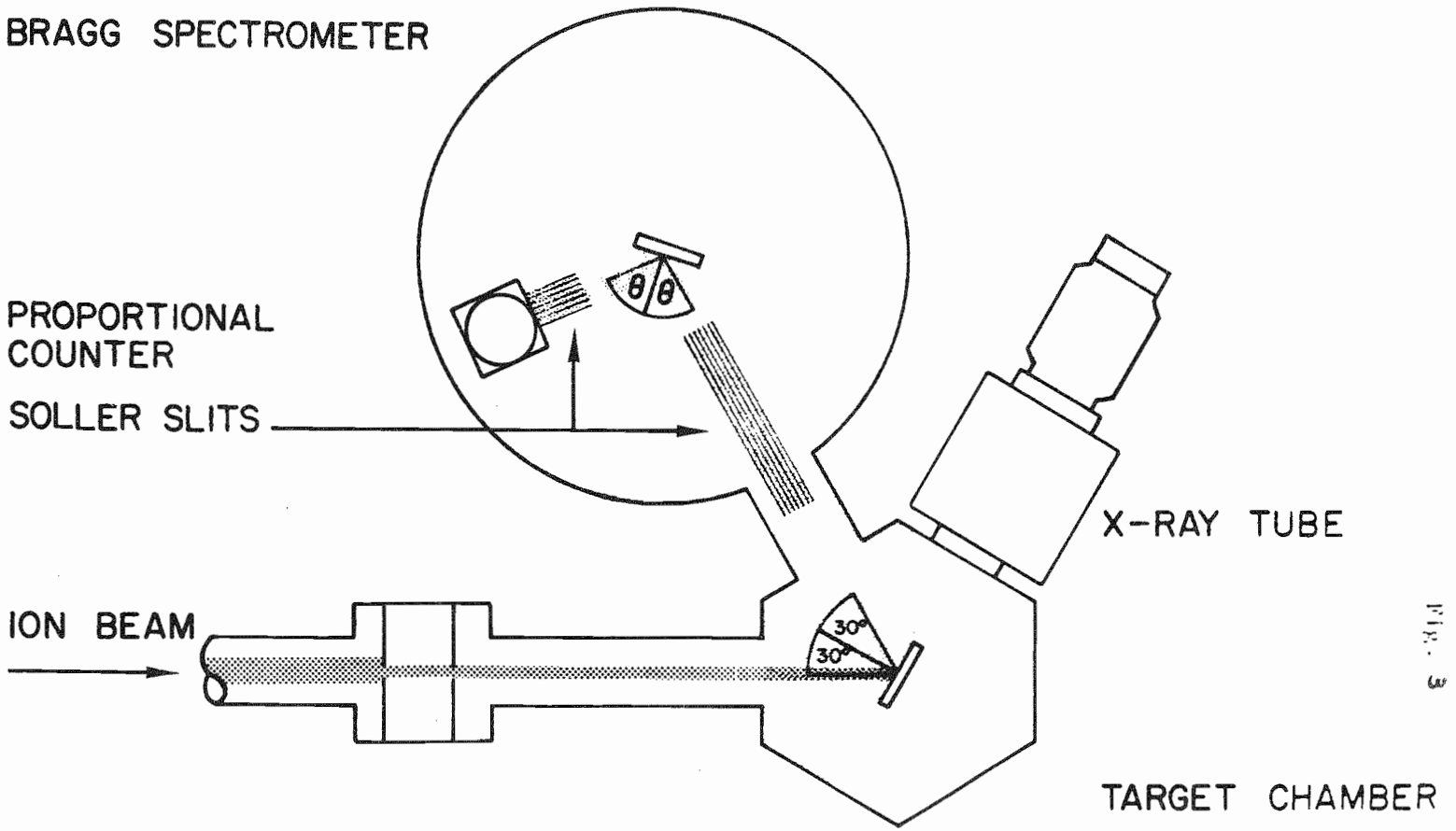
BRAGG SPECTROMETER
PROPORTIONAL COUNTER
SOLLER SLITS
θ θ
X-RAY TUBE
ION BEAM
30°
30°
TARGET CHAMBER

Fig. 4

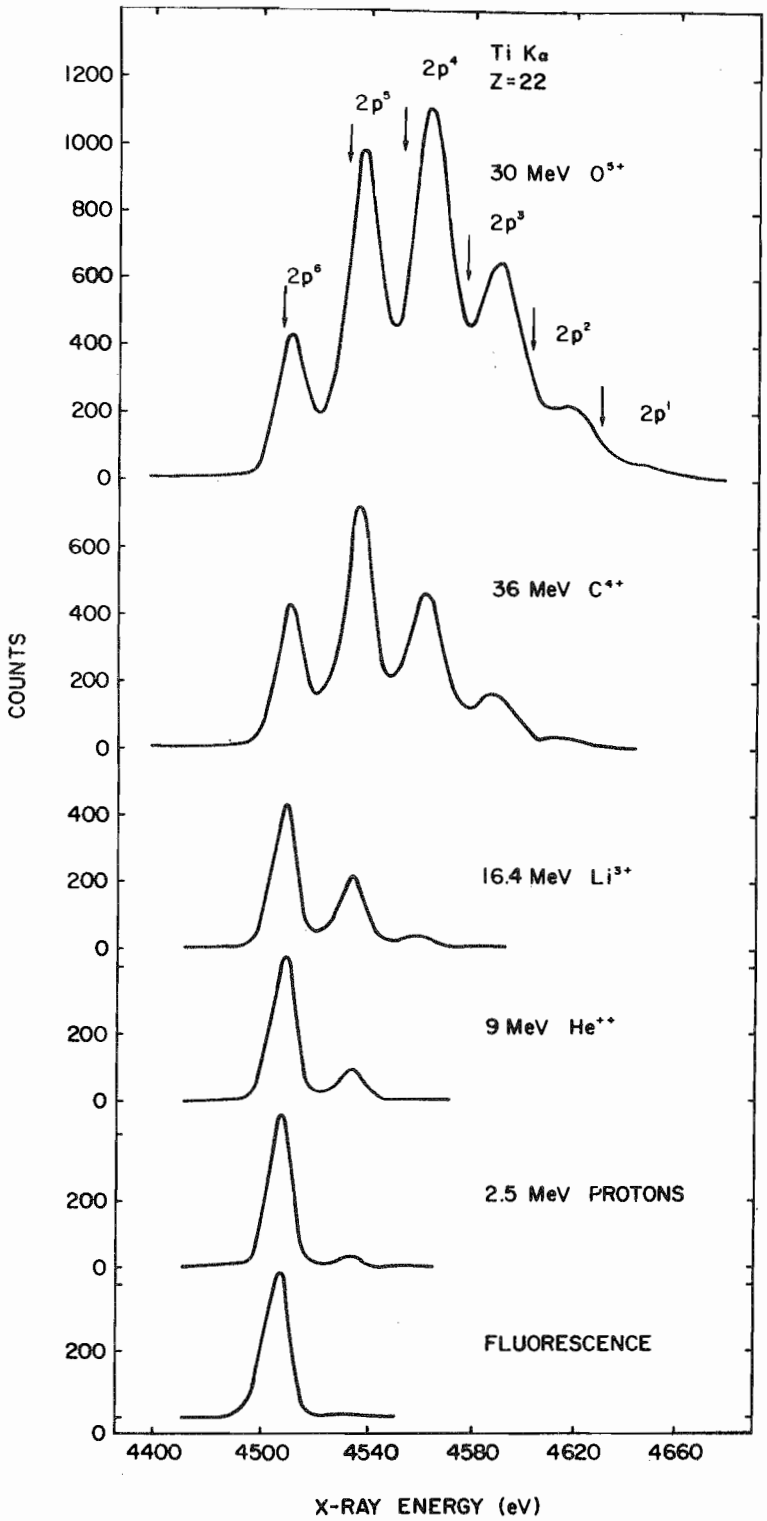
Ti Kα
Z=22
2p⁴
2p⁵
2p⁶
2p³
2p²
2p¹
30 MeV O⁵⁺
36 MeV C⁴⁺
16.4 MeV Li³⁺
9 MeV He⁺⁺
2.5 MeV PROTONS
FLUORESCENCE
COUNTS
X-RAY ENERGY (eV)
4400
4500
4540
4580
4620
4660

Fig. 5

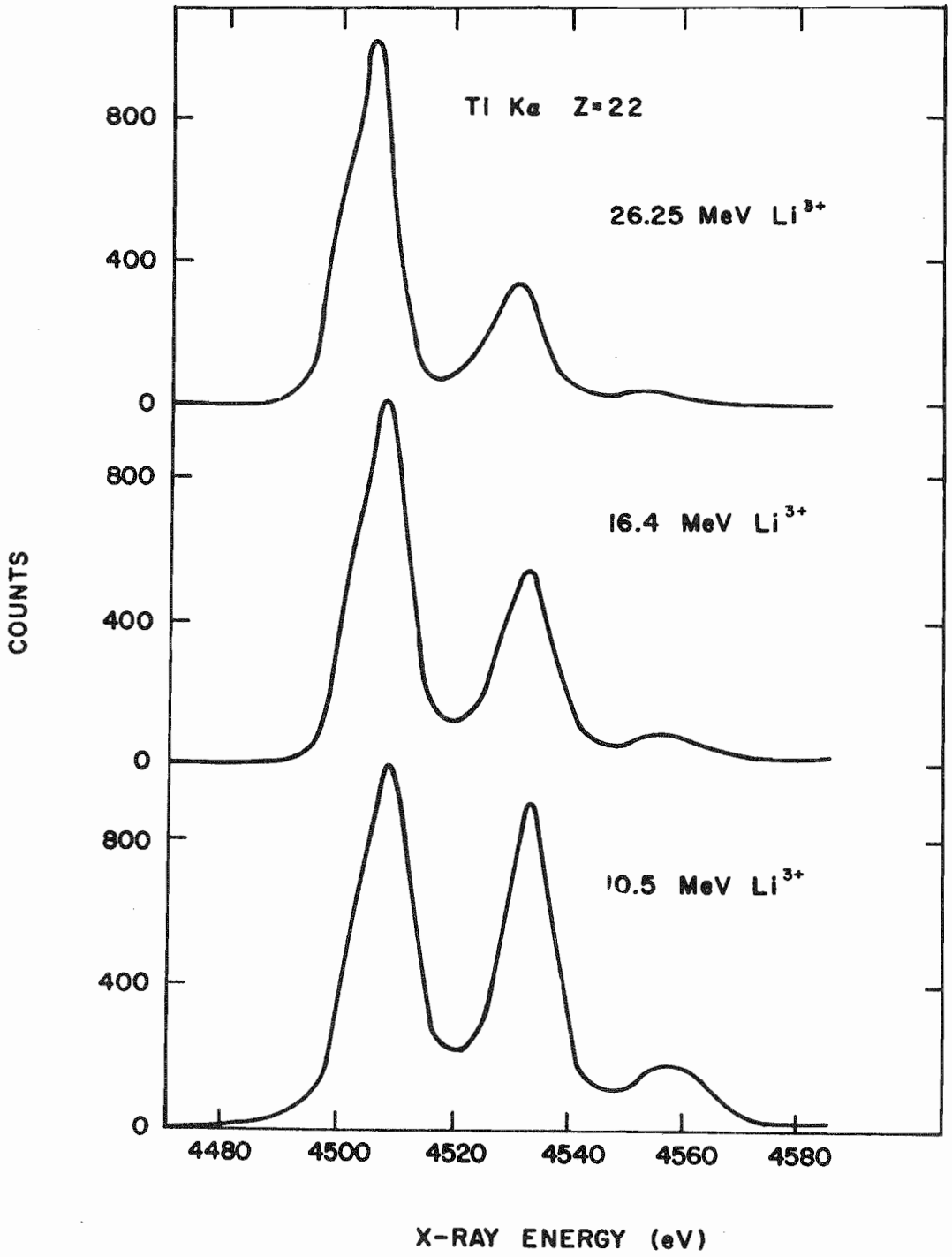
Ti Kα Z=22
26.25 MeV Li3+
16.4 MeV Li3+
10.5 MeV Li3+
800
400
0
800
400
0
800
400
0
COUNTS
4480
4500
4520
4540
4560
4580
X-RAY ENERGY (eV)

Fig. 6

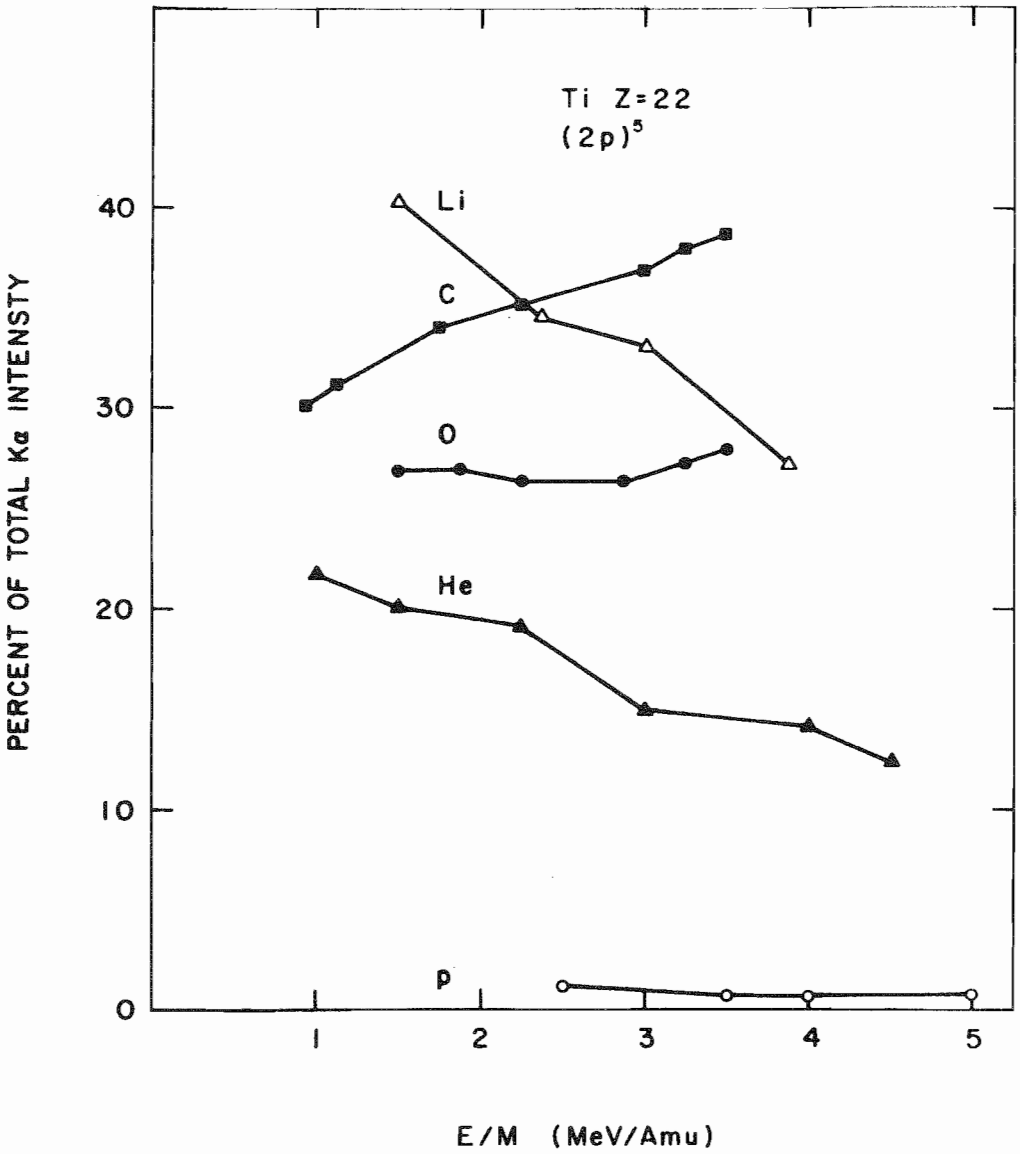
Ti Z=22
(2p)5
Li
C
O
He
p
40
30
20
10
0
1
2
3
4
5
PERCENT OF TOTAL Kα INTENSTY
E/M (MeV/Amu)

Fig. 7

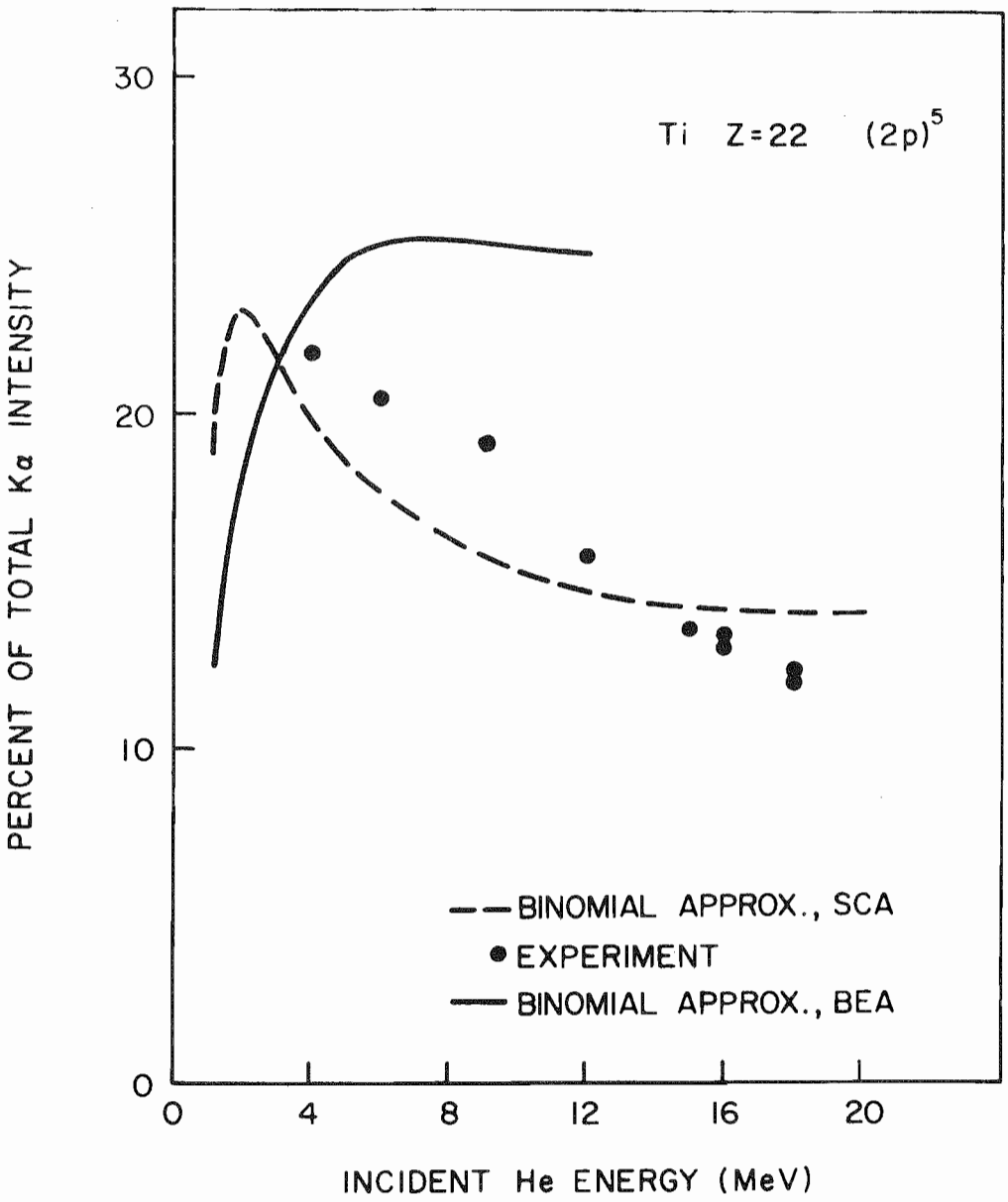
Ti Z=22 $(2p)^5$
PERCENT OF TOTAL Kα INTENSITY
INCIDENT He ENERGY (MeV)
BINOMIAL APPROX., SCA
EXPERIMENT
BINOMIAL APPROX., BEA
0
10
20
30
0
4
8
12
16
20

Fig. 8

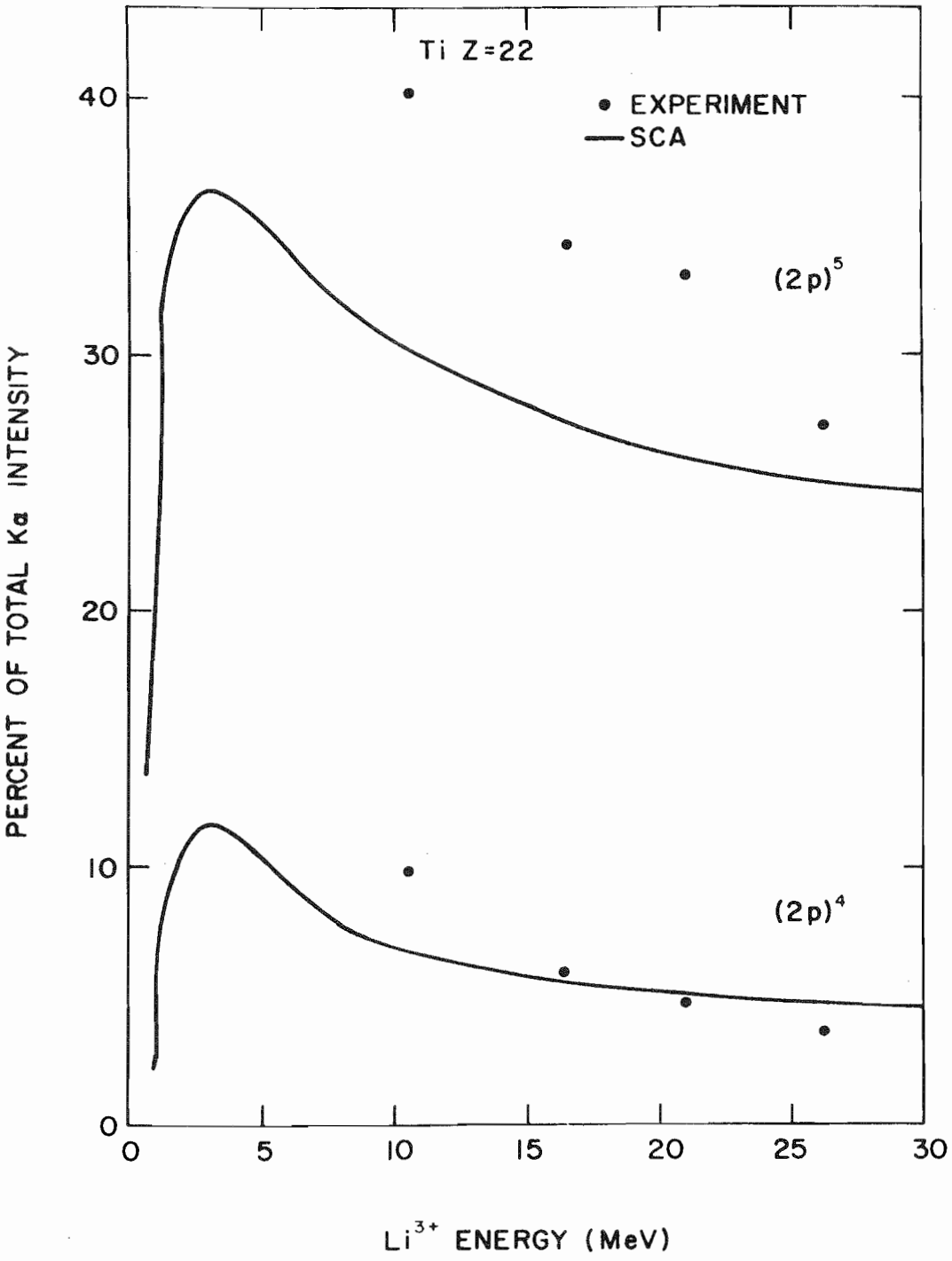
Ti Z=22
EXPERIMENT
SCA
$(2p)^5$
$(2p)^4$
PERCENT OF TOTAL Kα INTENSITY
Li^{3+} ENERGY (MeV)
0
10
20
30
40
0
5
10
15
20
25
30

Fig. 9

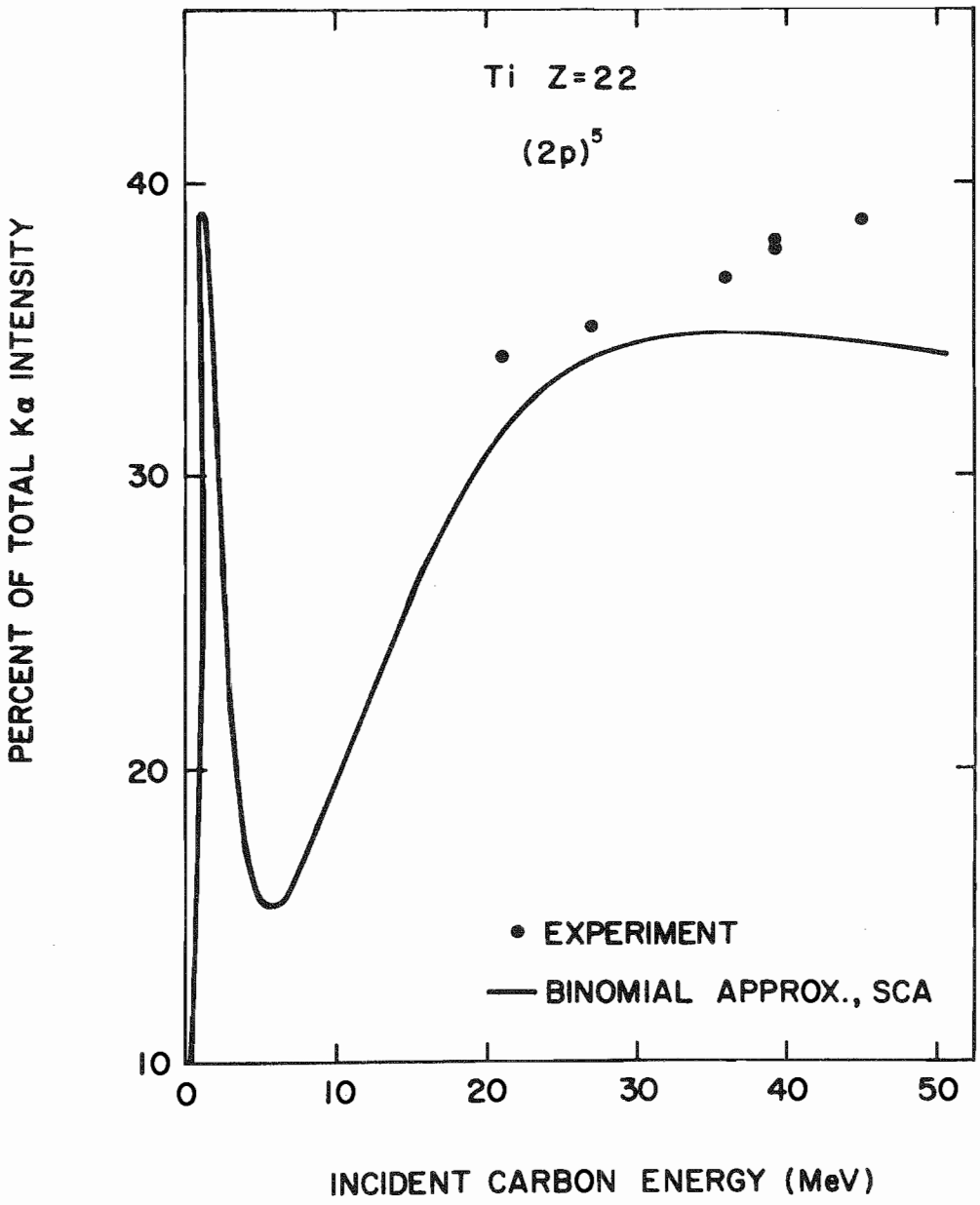
Ti Z=22
(2p)^5
PERCENT OF TOTAL Kα INTENSITY
40
30
20
10
0
10
20
30
40
50
• EXPERIMENT
— BINOMIAL APPROX., SCA
INCIDENT CARBON ENERGY (MeV)

Fig. 10

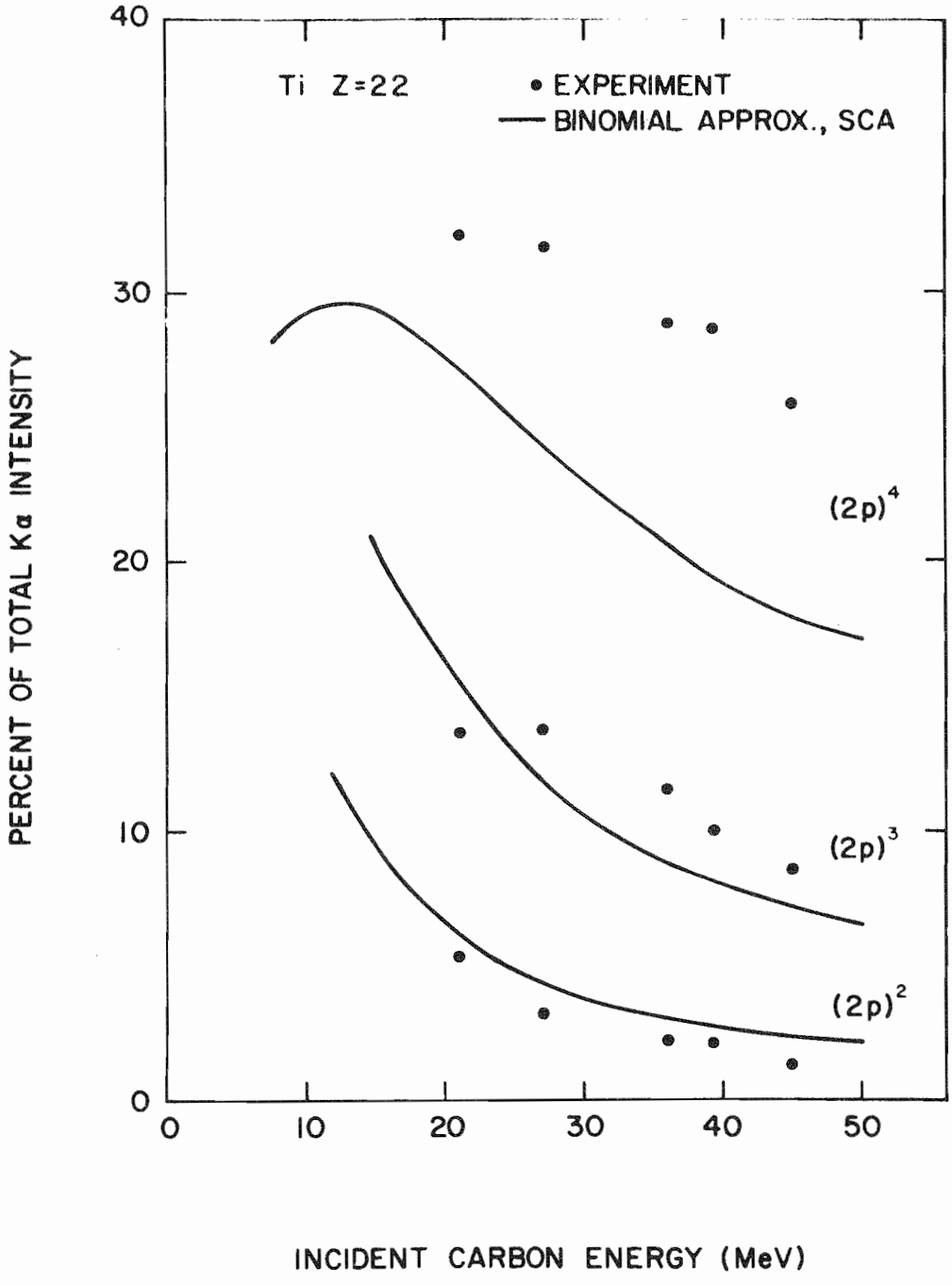
Ti Z=22
• EXPERIMENT
— BINOMIAL APPROX., SCA
(2p)^4
(2p)^3
(2p)^2
PERCENT OF TOTAL Kα INTENSITY
INCIDENT CARBON ENERGY (MeV)
0
10
20
30
40
50

Fig. 11

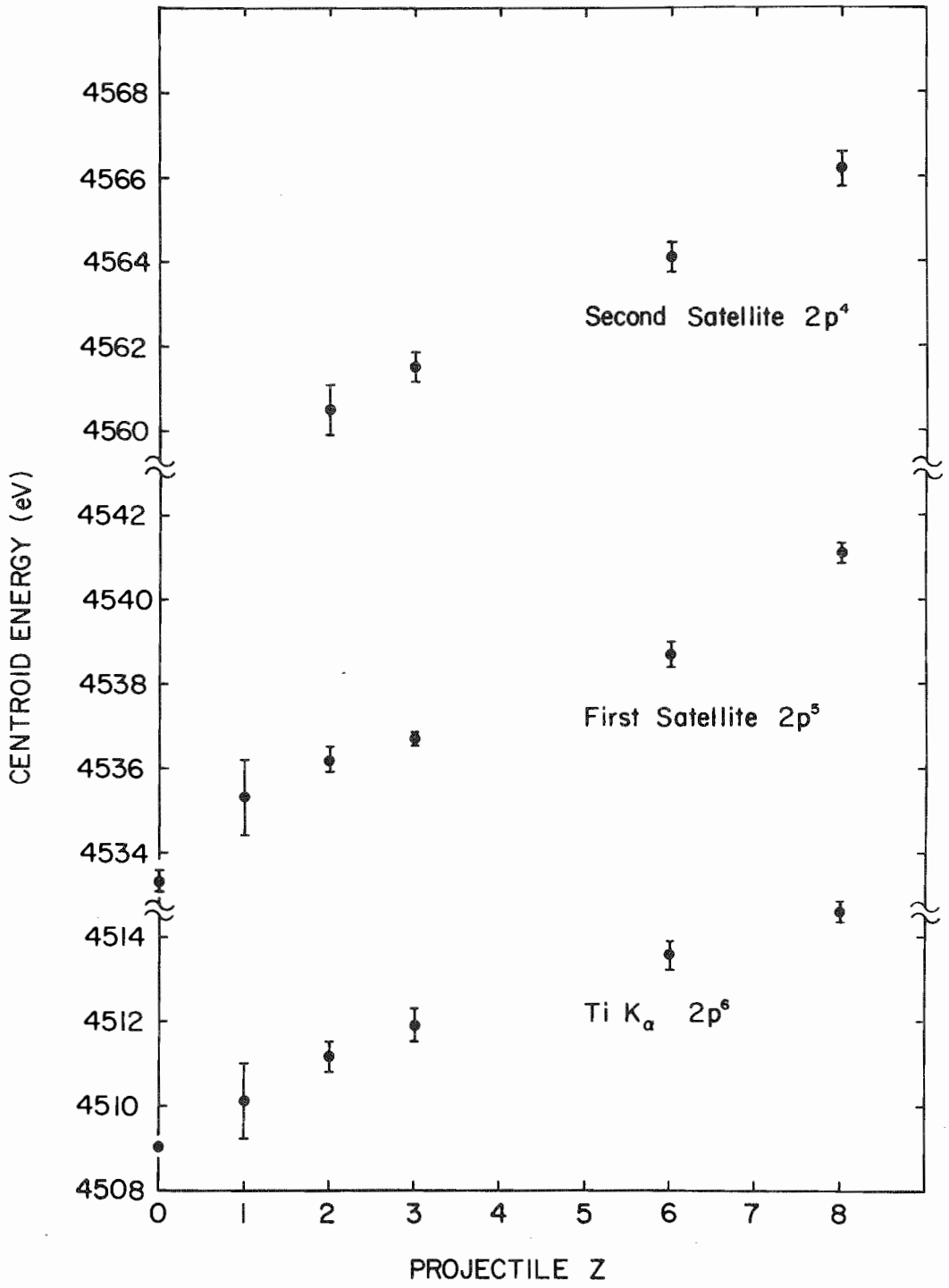
4568
4566
4564
4562
4560
4542
4540
4538
4536
4534
4514
4512
4510
4508
CENTROID ENERGY (eV)
Second Satellite 2p⁴
First Satellite 2p⁵
Ti Kα 2p⁶
0
1
2
3
4
5
6
7
8
PROJECTILE Z

Fig. 12

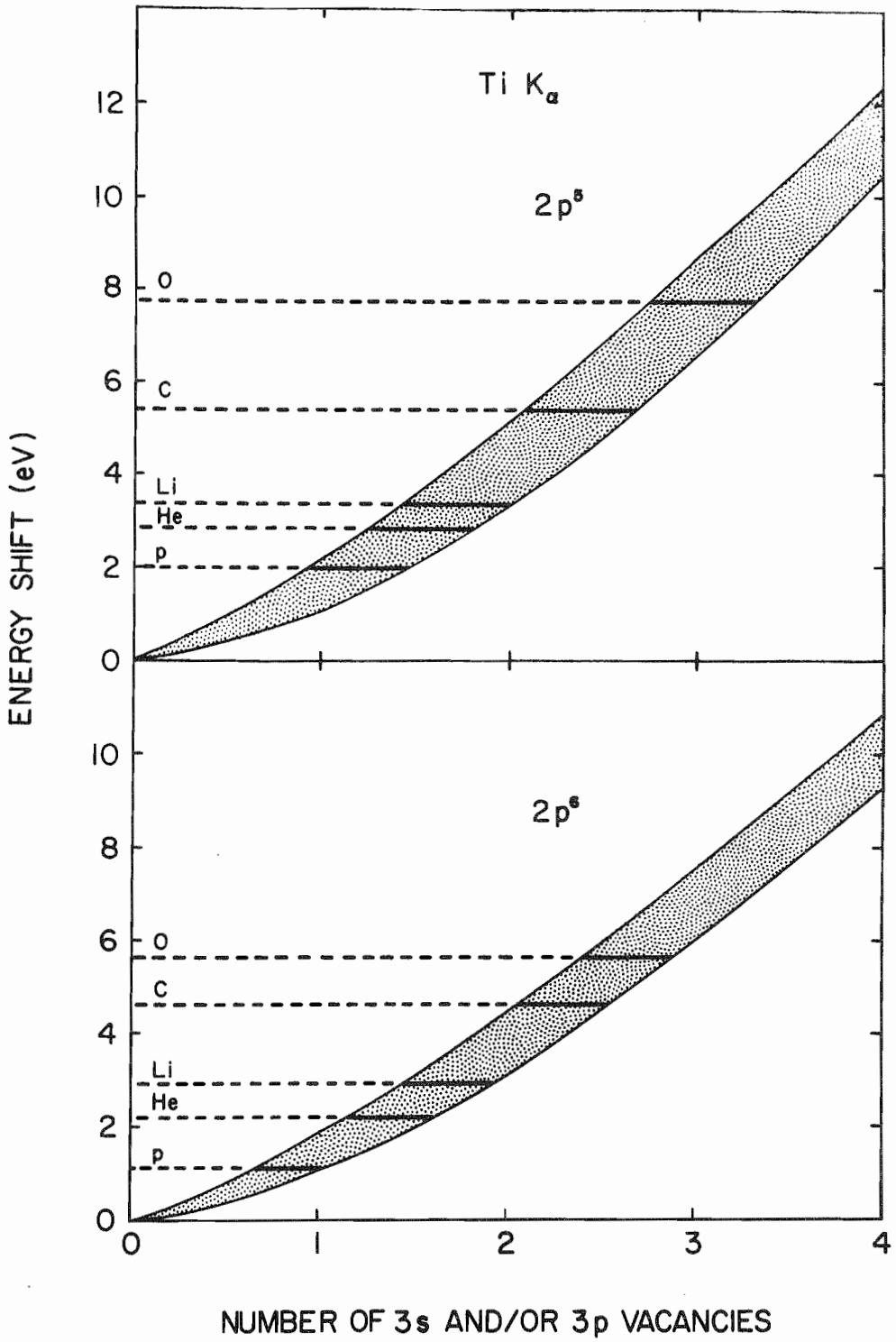
Ti K_α
$2p^5$
$2p^6$
O
C
Li
He
p
ENERGY SHIFT (eV)
NUMBER OF 3s AND/OR 3p VACANCIES
0
2
4
6
8
10
12
0
1
2
3
4